creative commons

COMMONS DEED

저작자표시-비영리-변경금지 2.0 대한민국

이용자는 아래의 조건을 따르는 경우에 한하여 자유롭게

- 이 저작물을 복제, 배포, 전송, 전시, 공연 및 방송할 수 있습니다.

다음과 같은 조건을 따라야 합니다:

저작자표시. 귀하는 원저작자를 표시하여야 합니다.

비영리. 귀하는 이 저작물을 영리 목적으로 이용할 수 없습니다.

변경금지. 귀하는 이 저작물을 개작, 변형 또는 가공할 수 없습니다.

- 귀하는, 이 저작물의 재이용이나 배포의 경우, 이 저작물에 적용된 이용허락조건을 명확하게 나타내어야 합니다.
- 저작권자로부터 별도의 허가를 받으면 이러한 조건들은 적용되지 않습니다.

저작권법에 따른 이용자의 권리는 위의 내용에 의하여 영향을 받지 않습니다.

이것은 이용허락규약(Legal Code)을 이해하기 쉽게 요약한 것입니다.

Disclaimer

dCollection

Ph.D. Dissertation of Biological Science

Genetic dissection of the selective autophagy network during senescence

세포 노화를 조절하는 선택적 오토파지의 네트워크 규명 연구

August 2023

School of Biological Sciences
Seoul National University

Yeonghyeon Lee

Genetic dissection of the selective autophagy network during senescence

Advisor
Professor Chanhee Kang, Ph.D.

A Thesis for the Degree of Doctor of Philosophy
June 2023

Seoul National University
School of Biological Sciences
Yeonghyoen Lee

Confirming the Ph.D. Dissertation written by
Yeonghyeon Lee
June 2023

Chair	김 진 홍	(Seal)
Vice Chair	강 찬 희	(Seal)
Examiner	고 준 석	(Seal)
Examiner	이 현 우	(Seal)
Examiner	신 동 혁	(Seal)

ABSTRACT

Yeonghyeon Lee
School of Biological Sciences
The Graduate School
Seoul National University

Cellular senescence is a complex stress response implicated in aging. Autophagy can suppress senescence but is counterintuitively necessary for full senescence. Although its anti-senescence role is well described, to what extent autophagy contributes to senescence establishment and the underlying mechanisms is poorly understood. Here, we show that selective autophagy of multiple regulatory components coordinates the homeostatic state of senescence. We combined a proteomic analysis of autophagy components with protein stability profiling, identifying autophagy substrate proteins involved in several senescence-related processes. Selective autophagy of KEAP1 promoted redox homeostasis during senescence. Furthermore, selective autophagy limited translational machinery components to ameliorate senescence-associated proteotoxic stress. Lastly, selective autophagy of TNIP1 enhanced senescence-associated inflammation. These selective autophagy networks appear to operate *in vivo* senescence during human osteoarthritis. Our data highlight a caretaker role of autophagy in the stress support network of senescence through regulated protein stability and unravel the intertwined relationship between two important age-related processes.

Keyword : Cellular senescence, Selective autophagy, Stress response, Oxidative stress, Proteostasis, Inflammation

Student Number : 2018-25197

CONTENTS

ABSTRACT i

CONTENTS ii

LIST OF FIGURES iii

INTRODUCTION 1

MATERIALS AND METHODS 9

RESULTS 23

DISCUSSION 72

REFERENCES 78

국문 초록 / ABSTRACT IN KOREAN 89

LIST OF FIGURES

Figure 1. Schematic representation of selective autophagy substrates identification platform during senescence.

Figure 2. Expression of SASP and $p16^{INK4a}$ changes during senescence

Figure 3. Venn diagrams summarizing autophagy interactome during cellular senescence

Figure 4. Heatmap representation of senescence-associated autophagy interactome (SAAI)

Figure 5. GO term analysis of the SAAI proteins

Figure 6. Determination of protein stability of 39 SAAI proteins using the GPS system.

Figure 7. Determination of protein stability of class I SAAI proteins upon the induction of bulk autophagy

Figure 8. Functional characterization of Class I SAAI proteins in the senescence regulatory network

Figure 9. Autophagy selectively targets KEAP1, eIF3 complex components, and TNIP1 for degradation in senescence

Figure 10. KEAP1 is a target of p62-mediated selective autophagy in senescence

Figure 11. NRF2 pathway is activated in senescence

Figure 12. Selective autophagy of KEAP1 activates the NRF2 pathway and promotes oxidative stress resistance

Figure 13. eIF3 complex is a target of NDP52-mediated selective autophagy in senescence

Figure 14. Selective autophagy of eIF3 limits protein translation and maintains proteostasis during senescence

Figure 15. Selective autophagy of eIF3 support senescent cell from proteotoxic stress for cell viability and SASP

Figure 16. TNIP1 is a target of OPTN-mediated selective autophagy in senescence

Figure 17. TNIP1 colocalizes with lysosome and OPTN

Figure 18. Selective autophagy of TNIP1 enhances senescence-associated inflammation during senescence

Figure 19. Selective autophagy of TNIP1 primes the paracrine senescence activity of senescent cells

Figure 20. KEAP1, eIF3, TNIP1 expression decreases during human osteoarthritis progression

Figure 21. Chondrocytes expressing a higher level of $p16^{INK4a}$ protein display decreased expression of KEAP1 and eIF3B proteins

Figure 22. KEAP1, eIF3 components, and TNIP1 proteins are regulated at the post-transcriptional level during in vivo senescence with human OA progression

Figure 23. Model of How Selective Autophagy Coordinates the Homeostatic State of Senescence Through Regulated Protein Stability

INTRODUCTION

Aging is characterized by the gradual deterioration of tissue function and is closely associated with several chronic human diseases (Lopez-Otin et al., 2013). For example, aging significantly increases the risk of cancer, cardiovascular disease, neurodegenerative disordes, osteoporosis, osteoarthritis, and metabolic syndrome (Campisi, 2013; Childs et al., 2015; Munoz-Espin and Serrano, 2014). These chronic diseases are the leading causes of morbidity and mortality, and extensive research has focused on treating them to improve human health. Targeting individual chronic diseases has had some success, leading to increased life expectancy. However, the complex and unique pathological nature of each disease makes it virtually impractical to cure or even treat them individually, which would require very high costs (Campisi et al., 2019). Therefore, there is an urgent need for a more efficient and cost-effective approach to treating multiple chronic diseases at once; targeting the aging process itself could be one such solution.

To address this challenging task, we should first define what the fundamental aging process is and then develop a strategy to target such a process. Although our knowledge is still incomplete, significant progress has been made recently in defining the hallmarks of aging (Childs et al., 2015; 2017; He and Sharpless, 2017; McHugh and Gil, 2018; Niedernhofer and Robbins, 2018; van Deursen, 2019). These include cellular senescence, a cellular aging process mainly characterized by irreversible growth arrest and secretion of many pro-inflammatory factors [i.e., the senescence-associated secretory phenotype (SASP)] (Kuilman et al., 2010;

Munoz-Espin and Serrano, 2014; Salama et al., 2014). Senescent cells accumulate in various tissues of different mammals, including humans, with age. They are also produced during the pathological progression of many age-related diseases. These observations led to the key hypothesis that senescence contributes to aging and that eliminating senescent cells could potentially delay the aging process.

In fact, a seminal study by the van Deursen group provided the first genetic evidence for the causal role of senescence in modulating aging and age-related diseases (Baker et al., 2011; 2016). They developed a mouse model called "INK-ATTAC" in which a fraction of senescent cells can be eliminated by drug-inducible caspase activation driven by a $p16^{INK4A}$ promoter, a well-established *in vivo* marker of senescence. The elimination of senescent cells had remarkable effects, ameliorating several age-related pathologies, including lipodystrophy, glomerulosclerosis, heart hypertrophy, and cataracts, and extending the lifespan of both progeroid mice and naturally aged mice (Baker et al., 2011; 2016). These studies have opened a new avenue for aging research, "senotherapy", which focuses on developing therapeutic strategies that target the detrimental effects of senescence to extend healthspan. A deeper understanding of senescence is therefore critical to advancing this important goal.

Senescence is a stress-activated genetic program that permanently arrests the proliferation of damaged cells and acts as a potent tumor suppressive mechanism (Childs et al., 2015; Kuilman et al., 2010; Lopez-Otin et al., 2013; Munoz-Espin and Serrano, 2014). While initially recognized as a response to telomere shortening due to replicative exhaustion, it has been found that various stresses, including DNA damage, oxidative stress, and oncogenic stress, can also induce senescence. Senescent cells exhibit additional features, such as altered morphology, changes in

chromatin structure (senescence-associated heterochromatin formation or SAHF), and the SASP. Of these, the SASP includes cytokines, chemokines, proteases, growth factors, and extracellular matrix components that collectively affect both senescent cells themselves and their tissue microenvironment, thereby mediating the pleiotropic effects of senescence. For example, Under physiological conditions, the SASP coordinate optimal tissue repair by promoting cell cycle arrest of damaged cells, their immune clearance, and stimulation of proliferation of neighboring normal cells. When dysregulated, however, it can contribute to chronic inflammation, tumorigenesis, and age-related diseases (Childs et al., 2015; Coppe et al., 2010; He and Sharpless, 2017; Soto-Gamez and Demaria, 2017; Tchkonia et al., 2013). Therefore, either eliminating the source of the SASP (i.e., senescent cells) or modulating the SASP, known as senotherapy, holds great promise for the treatment of aging (Childs et al., 2017; Kang, 2019; Kirkland and Tchkonia, 2017; van Deursen, 2019). How can we specifically target senescence and the SASP?

Senescent cells constantly experience multiple cellular stresses, including genome instability, oxidative stress, proteotoxic stress, and dysregulated metabolism; thus, they require the activation of cytoprotective stress responses to ensure their survival. Interestingly, many cancers share similar characteristics, and a decade of research has made significant progress in harnessing them for cancer treatment. This “non-oncogene addiction” strategy is based on the fact that the maintenance of the tumorigenic state relies on the activities of stress response pathways that are not inherently oncogenic. By targeting these pathways, cancer cells can be rendered vulnerable with minimal damage to normal cells. It is reasonable to apply the similar therapeutic strategy to senescence to effectively treat aging. For example, inhibition of the ubiquitin-

proteasome system (UPS) specifically sensitized cancer cells over their normal counterparts because cancer cells often experience higher levels of proteotoxic stress due to aneuploidy and copy number variation (Luo et al., 2009b). Similarly, gene expression profiling of senescent cells has revealed their dependence on pathways involved in Golgi vesicle trafficking, autophagy, and the UPS (Hernandez-Segura et al., 2017). Recent studies have shown that inhibition of autophagy sensitizes therapy-induced senescent cells to undergo apoptosis via endoplasmic reticulum-related mechanisms (Dorr et al., 2013). Investigating and targeting other stress support pathways in senescent cells may provide new avenues for exploiting such a "non-senescence addiction" for senotherapy.

In fact, this concept led to the development of the first generation of senolytics, drugs that selectively eliminate senescent cells. Senescent cells often increase the expression of pro-survival pathways, such as the anti-apoptotic B-cell lymphoma 2 (BCL2) protein family and dependence receptors/tyrosine kinases, to resist apoptosis. Targeting these anti-apoptotic pathways sensitized senescent cells to apoptosis, resulting in their relatively specific removal from tissues and ameliorating age-related diseases in mice, including cancer metastasis, idiopathic pulmonary fibrosis, atherosclerosis, cirrhosis, glomerulosclerosis, diabetes, sarcopenia, and osteoarthritis (Demaria et al, 2017; Schafer et al., 2017; Childs et al., 2016; Krizhanovsky et al., 2008; Ogrodnik et al., 2017; Valentijn et al., 2018; Thompson et al., 2019; Xu et al., 2018; Jeon et al., 2017).

Despite these promising results, current senolytic treatments have limitations. They eliminate not only the deleterious effects of senescent cells, but also their beneficial effects. Cellular senescence plays a role in wound healing, cellular reprogramming,

and tissue regeneration, suggesting that complete elimination of senescent cells may impede these beneficial effects (Demaria et al., 2014; Mosteiro et al., 2016; Ritschka et al., 2017). Furthermore, not all senescent cells lose their biological functions, suggesting that their maintenance may be necessary under certain conditions. For example, senescence of pancreatic β-cells increases their insulin secretion, which compensates for their decreased proliferation during aging (Helman et al., 2016). Therefore, the induction of senescence itself is not the problem, but rather the accumulation of senescent cells and their subsequent deleterious effects if not eliminated. To target senescent cells more safely, it may be more effective to modulate the senescence-supporting pathways that maintain the senescent state, rather than eliminating the senescent cells themselves. However, the other stress support pathways activated in senescent cells and their regulation remain largely unexplored.

Macroautophagy, also known as autophagy, is a crucial pathway for maintaining cellular homeostasis through lysosomal degradation. It involves the engulfment of cytoplasmic material by a double-membrane vesicle, the autophagosome, which then fuses with a lysosome for degradation and recycling. Initially identified through genetic screens in yeast, the core autophagy machinery consists of over 30 autophagy-related genes (ATGs) that are primarily responsible for autophagosome formation. This regulatory mechanism has expanded to include different types of autophagy that operate under specific conditions contributing to the autophagy regulatory network (Levine & Klionsky, 2004; Levine & Kroemer, 2019).

Autophagy can be divided into two types based on cargo specificity: bulk autophagy and selective autophagy. In bulk autophagy, materials for recycling are randomly selected for

degradation. In contrast, selective autophagy uses autophagy receptors that specifically target cargo to autophagosomes through interactions with core components of the autophagy machinery known as the ATG8 family of proteins. These proteins are also involved in cargo recognition during bulk autophagy (Gatica et al., 2018; Johansen and Lamark, 2020). Over the past decade, several cellular targets for selective autophagy have been identified, focusing primarily on large cellular structures associated with damage to maintain homeostasis, such as damaged mitochondria (mitophagy) and protein aggregates (aggrephagy) (Anding and Baehrecke, 2017; Galluzzi et al., 2017; Miller and Thorburn, 2021). Recent studies have shown that selective autophagy can also regulate the degradation of individual proteins in a controlled manner, similar to the ubiquitin-proteasome system (UPS), to modulate the stress response (Kwon et al., 2017; Sánchez-Martín and Komatsu, 2020). However, our understanding of autophagy substrate proteins and their physiological roles remains limited, mainly due to the lack of versatile systems to systematically identify and characterize them, unlike many UPS substrates (Iconomou and Saunders, 2016).

The relationship between senescence and autophagy is complex and not yet fully understood (Chan and Narita, 2019; Kwon et al., 2017; Leidal et al., 2018). Autophagy is required for many interventions that promote lifespan extension in various model organisms (Leidal et al., 2018; Levine and Kroemer, 2019). Initially reported as a quality control system that suppresses senescence, autophagy can be activated by various stresses that also induce cellular senescence. Autophagy can be activated by a variety of stresses including those that cause cellular senescence. For example, oxidative stress, the DNA damage response (DDR), the unfolded protein response (UPR), hypoxia, and inflammation can

potently activate autophagy through various signaling transducers (Kroemer, Marino, & Levine, 2010). Autophagy acts to maintain cellular homeostasis and suppress senescence in a passive manner before senescence is induced. It accomplishes this by targeting dysfunctional mitochondria and protein aggregates for degradation to maintain redox homeostasis and proteostasis. Autophagy also ensures lysosomal integrity and resolves stress granules. Additionally, autophagy can directly target critical regulators of senescence, such as GATA4, a key regulator of the senescence-associated secretory phenotype (SASP), through p62-dependent selective autophagy, thereby suppressing the SASP and senescence (Kang & Elledge, 2016).

Paradoxically, autophagy is activated during senescence and plays a crucial role in its establishment. Once senescence is triggered, autophagy functions as a "non-senescence addiction," where autophagy becomes necessary for senescence without inducing senescence itself. Autophagy dampens various senescence-associated stresses, thereby maintaining the viability of senescent cells (Kwon et al., 2017). Moreover, autophagy provides amino acids to support the massive synthesis of SASP factors through the formation of the TASCC complex (Narita et al., 2011). Autophagy can actively induce senescence by targeting negative regulators of senescence for degradation, such as Δ133p53α (an alternative splicing form of p53), Lamin B1 (a nuclear lamina component), and the histone deacetylase SIRT1 (Horikawa et al., 2014; Dou et al., 2015; Xu et al., 2020). However, our knowledge regarding the mechanistic role of autophagy in promoting and maintaining the senescent state is still limited. Specifically, we lack sufficient understanding of the specific senescence regulatory proteins targeted by autophagy and the extent to which their autophagic degradation contributes to

senescence.

This research aims to delve into the field of autophagy during senescence induction, focusing on the identification and characterization of substrate proteins, in particular those involved in the stress support network. By investigating their regulatory functions and determining their physiological relevance, we aim to fill existing knowledge gaps regarding the impact of autophagy on senescence regulation. Previous studies have partially addressed this topic, but comprehensive systems to identify and characterize these proteins at the systemic level are lacking. Therefore, this study introduces an integrated platform that explores the emerging functional module of autophagy by identifying, validating and characterizing substrate proteins targeted by selective autophagy during senescence induction. In addition, we aim to expand the scope of selective autophagy by characterizing stress response regulatory proteins that may parallel the importance of the ubiquitin-proteasome system in senescence induction. The results of this research could revolutionize our understanding of stress response mechanisms involving protein degradation, potentially paving the way for targeted senotherapy and novel treatments for age-related pathologies. By unraveling the molecular switch that activates selective autophagy upon senescence induction, this study also provides invaluable insights into the cellular logic of senescence regulation, facilitating the development of targeted interventions for various age-related pathologies. In conclusion, this study plays a crucial role in expanding our knowledge of the role of autophagy in cellular senescence and provides opportunities for the development of innovative therapies. The identification and characterization of novel substrate proteins targeted by selective autophagy have significant implications for future research in this emerging field.

MATERIALS AND METHODS

Cell lines and senescence induction

Human diploid fibroblasts (IMR90) and human embryonic kidney cells (HEK−293T) were obtained from the American Tissue Type Collection. IMR90 cells were maintained in 3% O_2 and cultured in Dulbecco's modified Eagle's medium (DMEM) supplemented with 15% fetal bovine serum (FBS), penicillin/streptomycin, and 0.1 mM nonessential amino acids. HEK−293T cells were maintained in 5% CO_2 and cultured in Dulbecco's modified Eagle's medium supplemented with 10% FBS and penicillin/streptomycin. Senescence was induced by ionizing radiation (12 Gy), treatment with bleomycin (10 μg/ml for 24 h; Cayman Chemicals), or replicative exhaustion.

Retroviral vectors and siRNAs

Retroviral vectors used in this study were shRNAs targeting TNIP1, OPTN, NDP52, and ATG7 subcloned from the GIPZ Lentiviral shRNA library (Dharmacon) into either pMSCV−PM or pINDUCER 10 vectors (Kang et al., 2015). The shRNA targeting sequences are as follows: TNIP1 shRNA#1, AGGAAAGGACTCAAATGTC; TNIP1 shRNA#2, TGATGAGCAATGGCAACAA; OPTN shRNA#1, AGGGCTCAGATGGAAGTTT; OPTN shRNA#2, AGGCTTACCTTGTTCAAAG; NDP52 shRNA, AGGGAGATCAAGATAAGAC; ATG7 shRNA#1, AGCATCATCTTC−GAAGTGA; ATG13 shRNA#1, CGTCTGTAGAAGACTCTCA; ATG13 shRNA#2, TCGTTCATCATCTTCTCCA; firefly luciferase (used as a control)

shRNA, CCCGCCTGAAGTCTCTGATTAA. The following cDNAs used in this study were from the Ultimate ORF clones (Invitrogen): GABARAP, GABARAPL1, GABARAPL2, LC3A, LC3B, LC3C, NBR1, NDP52, OPTN, p62, FNIP1, YWHAE, RNF114, SNAP29, TNIP1, FLCN, KEAP1, MIF, MVP, SERPINE2, TRAF2, TXN, RPSA, NFATC4, FYCO1, EFHD2, DYNLL1, LIMD1, CAPRIN1, PJA2, TRAF3, SNRPD3, WARS, NIPSNAP1, PEX11B, CKAP4, PARP9, PRKCI, EEF1D, VHL, ELOB, and ELOC. The following cDNAs used in this study were from the Human ORFeome library V8.1: ACAP3, DTX3L, UTP14C, HNRNPDL, NIPSNAP2, and UST. The cDNAs were subcloned into the following vectors (Kang et al., 2015): p-HAGE-GPS3.0-DEST vector, pMSCV vectors, pINDUCER20 vector, or pINDUCER20-N-term-Flag vector (which was generated in this study). siRNAs were transfected into cells at 20 nM for the individual siRNA and 50 nM for pools using Lipofectamine RNAiMAX transfection reagents (Invitrogen) according to manufacturer instructions. The following siRNAs were used: firefly luciferase siRNA, CGUACGCGGAAUACUUCGAUU; OPTN siGENOME siRNA, Dharmacon, D-016269-04; p62 siGENOME siRNA, Dharmacon, D-010230-04; NDP52 siGENOME siRNA, Dharmacon, D-010637-17.

Retroviral and lentiviral production

Retroviral and lentiviral gene delivery was performed as described (Kang et al., 2015). Infected cells were selected using puromycin (2 μg/ml; Clontech) for 3 days, geneticin (200 μg/ml; Gibco) for 7 days, or blasticidin (10 μg/ml; Invitrogen) for 5 days. For co-infections, cells were sequentially selected.

Conditioned medium

Normal cells, senescent cells, and senescent cells expressing TNIP1 were incubated for 96 h in DMEM with 0.5% FBS. After incubation, the conditioned medium (CM) was collected, centrifuged, and filtered through a 0.45 μm syringe filter (Acrodisc). CM was mixed with DMEM 60% FBS in a proportion of 3 to 1 to generate CM containing 15% FBS. The normal cells were incubated with CM containing 15% FBS for 7~10 days to examine paracrine senescence.

Label-free quantitative Affinity-Purification LC-MS/MS analysis

Affinity purification

A panel of human fibroblasts carrying N-terminal Flag-HA tandem tagged ATG8 family proteins (a total of six: MAP1LC3A [also known as LC3A], LC3B, LC3C, GABARAP, GABARAPL1, and GABARAPL2) and four major p62/SQSTM1-like autophagy receptors (NBR1, NDP52 [also known as CALCOCO2], OPTN, and p62 [also known as SQSTM1]) was generated. Using a stress-induced senescence model (ionizing radiation; 12 Gy), normal control cells (NOR), cells at early stage of senescence (3 days after exposure to IR, SEN (E)), and fully senescent cells (7 days after exposure to IR, SEN (F)) were prepared for affinity purification. Three biological replicates for each bait at each stage of senescence (a total of 99 samples) were subjected to affinity-purification liquid chromatography with tandem mass spectrometry (AP-LC-MS/MS).

Protein digestion and peptide sample preparation

Co-immunoprecipitated samples eluted with 8 M urea in 50 mM ammonium bicarbonate (ABC) buffer were incubated for 1 h at 37 ° C for denaturation, and followed by reduction of disulfide bonds with 10 mM DTT for 1 h at 37 ° C and cysteine alkylation with 40 mM iodoacetamide for 30 min at 37 ° C in the dark. Samples were diluted with 50 mM ABC to a < 1 M of urea concentration and followed by trypsin (2 % (w/w); Thermo Fisher, MS grade) digestion at 37 ° C for overnight. The resulting digests were subjected to a desalting step using C18 SPE cartridges (Supelco). Prior to mass spectrometry analysis, dried samples were reconstituted with 25 mM ABC buffer.

Liquid chromatography and tandem mass spectrometry (LC-MS/MS) analysis

The peptide samples were analyzed on a Q-Exactive mass spectrometer (Thermo Scientific) coupled with nanoAcquity UPLC (Waters, Milford, MA), which was operated at a flow rate of 300 nL/min over 100 min with a linear gradient ranging from 95% solvent A (H_2O with 0.1% formic acid) to 40% of solvent B (acetonitrile with 0.1% formic acid). Analytical capillary column (100 cm x 75 μm i.d.) and trap column (3 cm x 150 μm i.d) were packed in-house with 3 μm Jupiter C18 particles (Phenomenex, Torrance, CA). The long analytical column was placed in a column heater (Analytical Sales and Services, Pompton Plains, NJ) maintained at a temperature of 45 ° C. Precursor ions were acquired at a range of m/z 400-1800 under 70 k resolution (at m/z 200). Top 10 precursors were subjected to MS/MS analysis at 2 Th of precursor isolation width. Higher-energy collisional dissociation

with 25% collision energy, a target value of 1E6 ions determined by automatic gain control, 60 ms maximum injection time, and 17.5 k resolution at m/z 200 were applied for MS/MS analysis.

LC-MS/MS data processing and protein identification

All 99 LC-MS/MS datasets were processed by MaxQuant (version 1.5.3.30) with Andromeda search engine at 20 ppm and 4.5 ppm precursor ion mass tolerance for the first search and main search, respectively, using the SwissProt Homo sapiens proteome database (20,386 entries, UniProt). The following search parameters were applied: fully tryptic digestion, fixed carbaminomethylation on cysteine, and dynamic oxidation of methionine. The false discovery rate was set at 1% for both peptide and protein group level by performing a decoy database search. The label-free quantification (LFQ) and match-between-runs options were used for protein quantification, where only the quantity of unique peptides were included for the extraction of protein LFQ intensity and proteins with ≥2 of unique peptides were finally reported as quantifiable proteins. Defined LFQ intensity values were log_2-transformed for further analysis.

Statistical processing of LFQ intensity data to determine the genuine interactors of bait proteins

All protein LFQ intensities from AP-LC-MS/MS datasets were normalized by the median values of individual protein groups across the whole AP-LC-MS/MS datasets. Student' s t-test between negative control and bait dataset at each condition (NOR, SEN (E), SEN (F)) was carried out based on the normalized LFQ intensities using Perseus software (Ver 1.6.2.3). First, proteins enriched in

the negative control datasets with p-value < 0.01 (unpaired two-tailed t-test) were considered as non-specific binders and not included for further analyses. Next, the potential interactors of bait proteins, which were enriched in the bait AP-LC-MS/MS datasets, were classified into three classes (class A, B and C) based on fold-change (FC, i.e., $\log_2$(bait/control)) and p-value: class C; all proteins with FC ≥ 1, class B; proteins with 1 ≤ FC < 4 and p-value < 0.01 among the class C proteins, class A: proteins with FC ≥ 4 and p-value < 0.01 among the class C proteins. In this study, the only proteins in class A were considered as genuine interactor candidates. To examine the changes in interaction during the progression of senescence, further normalization of MS intensities of interactors at each stage of senescence (NOR, SEN (E), SEN (F)) were normalized to those of bait proteins. Two-way ANOVA was used for the statistical analysis to determine interactors whose interaction with the baits change during the progression of senescence. GO term analysis was done after excluding ribosomal proteins (RPS2, RPS3, RPS3A, RPS4X, RPS5, RPS6, RPS7, RPS8, RPS10, RPS11, RPS13, RPS14, RPS19, RPS20, RPS23, RPS25, RPS26P11, RPS27A, RPL8, RPL13, RPL13A, RPL19, RPL23A, RPL24, RPL27A, RPL28, RPL31, RPL32, RPL35, RPL36AL, and RPLP1) and proteasome subunits (PSMA1, PSMA2, PSMA3, PSMA4, PSMA5, PSMA6, PSMA7, PSMB1, PSMB2, PSMB3, PSMB4, PSMB6, PSMC3, PSMC5, PSMC6, PSMD1, PSMD2, PSMD6, PSMD7, and PSMD11).

Gene expression profiling

Total RNAs were isolated using the acidic phenol extraction method. One microgram of high-quality RNA samples (RIN > 7.0) was used to construct RNA-seq libraries using the TruSeq Stranded mRNA

LT Sample Prep Kit (Illumina). Total RNA integrity was checked using an Agilent 2200 TapeStation. RNA-seq was performed on an Illumina NovaSeq 6000 sequencer at Macrogen. The sequence reads were trimmed with Trimmomatic and mapped against the human reference genome (hg38) using Hisat2. Read counts per gene were calculated by using featureCounts (Table S4). Differential expression analysis was conducted by using the DESeq2 R package. Genes with adjusted p-value < 0.05 and |fold-change| >1 were selected as differentially expressed genes (DEGs). The Database for Annotation, Visualization and Integrated Discovery (DAVID) v6.8 was used for GO term analysis (Table S5) (Huang da et al., 2009).

Gene set enrichment analyses

Gene set enrichment analyses (GSEA) was performed by using default setting: weighted enrichment statics and Signal2Noise metric for ranking genes (Subramanian et al., 2005). Additional transcriptome data used in this study for GSEA were GSE57218 (human OA transcriptome), GSE63577 (IMR90 replicative senescence transcriptome), and GSE77675 (WI-38 replicative senescence transcriptome). The NRF2 gene set (a total of 449 genes) was defined by merging antioxidant gene set (a total of 196 genes from the Harmonizome (Rouillard et al., 2016)) and NRF2_Q4 set (a total of 259 genes from the v7.4 TRAFSFAC). The SASP gene set was defined by selecting genes differentially expressed in irradiation-induced senescent fibroblasts (a total of 599 genes, q < 0.05) from the SASP atlas (Basisty et al., 2020). The complete lists of genes are presented in Table S6.

Quantitative RT−qPCR

Total RNAs were extracted using QIAzol lysis reagent (Qiagen), and cDNA was synthesized using ReverTra Ace® qPCR RT Master Mix (Toyobo) according to manufacturer's instructions. Quantitative RT−qPCR was performed in triplicate using SYBR TOPreal qPCR 2× preMIX (Enzynomics) on a QuantStudio5 PCR instrument (Applied Biosystems). GAPDH served as an endogenous normalization control. Primer sequences used in this study are listed in Table S7.

SA−β−galactosidase assay, BrdU incorporation assay, ROS decay analysis, and apoptosis assay

SA−β−galactosidase assay

SA−β−gal activity was determined using the C_{12}FDG staining kit according to manufacturer's instructions. Briefly, cells were pretreated with 100 nM bafilomycin A1 (Cayman Chemicals) for 1 h, and then incubated with 20 μM C_{12}FDG (Invitrogen) for 1 h. SA−β−gal activity was analyzed by FACS (Attune NxT Flow Cytometer, Thermo Fisher Scientific).

BrdU incorporation assay

Cells were plated on Lab−Tek II chamber slides and labeled with BrdU (10 μM, BD Science) for 4 h. Nuclei incorporating BrdU were visualized by immunofluorescence using an antibody to BrdU (BD Science) according to manufacturer instructions. The percent positive stained cells were determined as (number of positive cells) / (total number of cells) x 100 in 3 randomly selected area per

sample at 100X magnification.

ROS decay analysis

Cells were stained with 20 μM DCFDA (Invitrogen) for 45 min, and then incubated with 1 mM H_2O_2 for the indicated time. Median fluorescence of DCF was measured by FACS and normalized to the median value of normal control cells at 0 min.

Cell death assay

Cell death was analyzed by FACS using a FITC Annexin V Apoptosis Detection Kit I from BD Pharmingen or propidium iodide (PI) according to the manufacturer's instructions.

FACS analysis for GPS, Proteostat and protein synthesis

GPS

GPS analysis was performed as described (Emanuele et al., 2011). Briefly, FACS was used to partition the cells expressing the indicated GPS vectors into six bins of equal sizes based on the GFP/DsRed ratio. We then calculated the protein stability index (PSI) for each protein as described (Emanuele et al., 2011). The value of PSI ranged from 1-6, with a higher PSI value indicating higher relative protein stability of the indicated proteins. The ⊿PSI was calculated by subtracting the two PSI numbers (condition#1 - condition#2). A one-sample t-test was used for the statistical analysis to determine proteins whose stability changed during senescence and paired two-tailed t-test was used for the

statistical analysis to determine autophagy substrates.

Proteostat

Proteostat staining was performed using Proteostat Aggresome detection kit (Enzo Life Sciences) according to manufacturer' s instructions. Briefly, cells were pretreated with or without 10 μM MG-132 (Apexbio) for 18 h prior to fixation with 4% PFA in PBS for 30 min on ice. Cells were stained with Proteostat dye for 30 min at room temperature, and then analyzed by FACS. The median value of fluorescence was measured and normalized as follows to combine independent experiments: the minimum and maximum median values on the day of the measurement were set as 1 and 100, respectively.

Protein synthesis

Global protein synthesis was measured using the Click-iT AHA Alexa Fluor 488 Protein Synthesis HCS Assay (Thermo Fisher) according to the manufacturer' s protocol. Briefly, cells were incubated with L-methionine-free media to deplete methionine reserves prior to labeling with 100 μM L-azidohomoalanine (L-AHA) for 2 h. Cells were then trypsinized, fixed with 4% PFA in PBS for 20 min at room temperature, permeabilized with 0.5% Triton-X-100 in PBS for 20 min at room temperature, and incubated with click-it reaction mixture for 30 min prior to FACS analysis.

Polysome profiling

Cells were treated with Trypsin-EDTA containing freshly added

100 μg/mL of cycloheximide (Sigma) and resuspended in media containing 100 μg/mL of cycloheximide. Cells were collected by centrifugation at 1200 x g for 5 minutes at 4 ° C. Following a wash with PBS, the cells were incubated in 100 μl of the lysis buffer (20 mM Tris-HCl pH 7.5, 100 mM KCl, 5 mM $MgCl_2$, and 0.5% NP-40) for 30 min at 4 ° C with freshly added 100 μg/mL of cycloheximide, 0.5 μl of SUPERaseIn RNase inhibitor (1:200, Invitrogen), 1 μl of phosphatase inhibitor (1:100, AG Scientific), and 0.17 μl of protease inhibitor (1:600, Calbiochem). The lysate was centrifuged at 12,000 x g for 10 min at 4 ° C to remove the nuclei and cell debris. The supernatant was transferred to a new tube and the protein concentration was measured by BCA. A total of 400-500 μg lysate was loaded to the top of the sucrose gradient solution (10-50%) and centrifuged at 36,000 rpm for 2 h at 4 ° C. After the ultracentrifugation, the UV absorbance of the gradient was measured at 260 nm using a BioLogic LP system.

Human OA sample procurement and immunohistochemistry analysis

Human OA cartilage specimens were procured from OA patients undergoing total knee replacement at the SNU Boramae Medical Center in accordance with institutional guidelines governed by approved protocols (IRB nos. 26-2016-143 and 30-2017-48 for the collection of materials; IRB No. E1803/003-009 for the use of materials). The formalin fixed paraffin-embedded tissue sections were deparaffinized and rehydrated. The slides were incubated in Tris-EDTA buffer (pH 9.0) for 2 h at 60 ° C, washed with TBS, and blocked with 1% bovine serum albumin in TBS. The slides were incubated with the indicated primary antibodies overnight at 4 ° C, washed 3 times with TBS, and incubated with Alexa Fluor

conjugated secondary antibodies for 1 h at room temperature. The nuclei were stained with DAPI. Images were obtained by LSM 700 laser scanning confocal microscopy. The fluorescence intensity of each cell was measured using ImageJ software (NIH).

Immunoprecipitation, Western blotting, immunofluorescence

Immunoprecipitation

Cells were harvested and lysed in NP-40 lysis buffer. Anti-Flag-conjugated magnetic beads (Sigma) or anti-HA-conjugated magnetic beads (Thermo Fisher) were used to enrich bait proteins. An equal amount of protein lysates was subjected to affinity-purification for 2 h at 4 °C. For endogenous co-immunoprecipitation, lysates were preincubated with the indicated antibodies for overnight at 4 ° C and subsequently incubated with Dynabeads Protein G (Invitrogen) for 1 h at 4 ° C. Beads were washed six times with NP-40 lysis buffer and proteins bound to the beads were eluted with 2× Laemmli sample buffer and subjected to SDS-PAGE.

Western blotting

Protein lysates were loaded onto the SDS-polyacrylamide gel and subjected to electrophoresis. After electrophoresis, the proteins were transferred to nitrocellulose membrane and subjected to immunoblotting with the indicated antibodies. Immunoblotting images were acquired by iBright CL1000 imaging system (Thermo Fisher). Immunoblotting signals were normalized to control (either VINCULIN or GAPDH) unless otherwise indicated.

Immunofluorescence

Cells were plated in the Lab-Tek II chamber slide (Thermo Fisher) and treated as indicated. Cells were fixed with 4% paraformaldehyde for 10 min at room temperature, washed three times with PBS, permeabilized with ice-cold PBS containing 0.5% Triton-X 100 in PBS for 10 min, washed with PBS, blocked with 3% bovine serum albumin in PBS-T (PBS with 0.1% Tween 20), and subjected to immunostaining with the indicated antibodies. DAPI was used to stain the nuclei. Images were obtained by LSM 700 laser scanning confocal microscopy. Colocalization analysis was performed using ImageJ software (NIH).

Antibodies

The primary antibodies used in this study were as follows: anti-VCL (Sigma), anti-GAPDH (Santa Cruz), anti-ACTB (Santa Cruz), anti-NDP52 (Abnova), anti-OPTN (Cayman), anti-p62 (BD Biosciences), anti-phospho-SQSTM1/p62 (Ser349) (Cell signaling), anti-FLAG (Sigma), anti-TNIP1 (Invitrogen), anti-KEAP1 (Proteintech), anti-eIF3B (Bethyl), anti-eIF3C (Bethyl), anti-eIF3D (Bethyl), anti-eIF3K (Novus), anti-eIF3L (GeneTex), anti-RPL13a (Cell signaling), anti-RPS6 (Cell signaling), anti-eIF4E (Cell signaling), anti-p70 S6 Kinase (Cell signaling), anti-Phospho-p70 S6 Kinase (Thr389), anti-p53 (Calbiochem), anti-p21 (Calbiochem), mono-and polyubiquitinylated conjugates monoclonal antibody (FK2) (Enzo), anti-p16 (BD Biosciences), anti-RELA (Santa Cruz), anti-p-RELA(S536) (Cell Signaling), anti-ATG13 (Cell signaling), anti-ATG7 (Cell Signaling), anti-IgG (Santa Cruz), anti-p16 (Abcam), anti-GATA4 (Santa Cruz), anti-LC3B (Cell Signaling), anti-OPTN (Proteintech), Alexa Fluor 488

conjugated anti-BrdU (BD Biosciences). HRP-conjugated anti-mouse IgG and anti-rabbit IgG secondary antibodies were obtained from the Jackson ImmunoResearch Laboratories Inc.

Quantification and statistical analysis

No statistical methods were used to predetermine sample sizes. Data met the assumptions of the statistical tests used. Data analyses were performed using Graph Pad Prism software (Graphpad Software Inc).

Data and code availability

Data supporting the findings of this study are available within paper, its supplementary figures and tables, and accession codes for analyzed public datasets are included in method details. The accession numbers for the proteomic and RNA-seq data reported in this paper are PRIDE: PXD024787 and GEO: GSE168994, respectively.

RESULTS

Autophagy Interactome during Cellular Senescence

To systematically discover autophagy substrate proteins (Figure 1), we first performed a proteomics screen to identify proteins showing alterations in their interaction with the ATG8 family proteins and several autophagy receptors during senescence, since they are key in cargo selection during autophagy (Gatica et al., 2018; Johansen and Lamark, 2020). We generated a panel of human fibroblasts carrying N-terminal Flag-HA tandem-tagged six ATG8 family proteins [LC3A (alias MAP1LC3A), LC3B, LC3C, GABARAP, GABARAPL1, and GABARAPL2] and four major p62/SQSTM1-like autophagy receptors [NBR1, NDP52 (alias CALCOCO2), OPTN, and p62 (alias SQSTM1)]. Using a stress-induced senescence model (Coppe et al., 2008), we prepared normal control cells (NOR), cells at an early stage of senescence [SEN (E)], and fully senescent cells [SEN (F)], as assessed by the expression of $p16^{INK4a}$ protein and several SASP genes (Figure 2). Three biological replicates for each bait at each stage of senescence (a total of 99 samples) were subjected to affinity-purification liquid chromatography with tandem mass spectrometry (AP-LC-MS/MS) (Behrends et al., 2010), and candidate proteins were stringently selected (Figure 1), referred to here as the senescence-associated autophagy interactome (SAAI).

We identified a total of 360 non-redundant proteins making 634 interactions in the SAAI (Figure 3) with high Pearson's correlation coefficients, indicating high reproducibility between biological triplicate samples. The SAAI revealed previously known interactions such as LC3B–FYCO and NDP52–TRAF2, as well as

recently identified autophagy substrate proteins such as KEAP1 and TRAF3 (Figure 4) (Komatsu et al., 2010; Newman et al., 2017; Olsvik et al., 2015; Rual et al., 2005). Gene ontology (GO) analysis of the SAAI showed significant enrichment in biological processes related to autophagy regardless of the stage of senescence, as expected (Figure 5). The term "canonical glycolysis" was enriched at the early stage, suggesting that autophagic regulation might contribute to changes in glycolysis during senescence progression (Wiley and Campisi, 2016). Furthermore, the term "spliceosome" was enriched at the full senescent stage, indicating that autophagy might be involved in senescence-associated splicing changes (Georgilis et al., 2018). Interestingly, the term "translation initiation" was also prominent at the full senescent stage, with several components of eukaryotic initiation factor 3 (eIF3) being recovered. This suggests that autophagy might modulate protein translation during senescence.

Autophagy Substrate Proteins that Modulate the Features of Senescence

To identify autophagy substrate proteins in the SAAI, we performed a focused genetic screening using the Global Protein Stability (GPS) system (Yen et al., 2008) to search for a protein for which stability was changed in an autophagy-dependent manner during senescence. Because we were mainly interested in autophagy substrate proteins that can control senescent features, we first categorized 360 protein candidates according to their cellular function based on the associated GO terms. Next, we selected proteins that are related to the following senescence-associated biological processes (Gorgoulis et al., 2019; Herranz and Gil, 2018): protein quality control, cancer, inflammation, metabolism,

oxidative stress, cellular trafficking, and RNA processing. Finally, we excluded proteins that function as part of a multi-protein complex because they tend to become unstable non-physiologically when ectopically expressed (Torres et al., 2010). Collectively, we selected a total of 39 proteins in the SAAI for protein stability profiling.

Of the 39 examined proteins, the stability of 17 proteins significantly decreased during senescence (Figure 6A; Figure 6B). Inhibition of autophagy increased the stability of 10 proteins (Figure 6A; hereafter, class I SAAI proteins), which could be divided into two subgroups. The first group showed reduced stability during senescence (a total of seven: senescence-regulated autophagy substrates); the second group did not exhibit changes in stability upon senescence induction (a total of three: senescence-independent autophagy substrates). The UPS or other protein degradation pathways might regulate the remaining proteins for which stability decreased during senescence in an autophagy-independent manner. The stability of the senescence-regulated class I SAAI proteins was not reduced upon the induction of bulk autophagy via mammalian target of rapamycin (mTOR) inhibition (Figure 7), suggesting specificity of their autophagic degradation during senescence. Together, these results suggest that our platform identified novel autophagy substrate proteins in senescence, as well as previously known ones.

Next, we determined whether class I SAAI proteins function in senescence by examining multiple senescence markers including senescence-associated β-galactosidase (SA-β-gal) activity, cell cycle arrest, and the activation of three main branches of the senescence regulatory network, namely the p53-p21, $p16^{INK4a}$, and SASP pathways (Hernandez-Segura et al., 2018). Ectopic expression of TNIP1, KEAP1, and UST increased SA-β-gal

activity (Figure 8A). TNIP1 expression decreased the activity of the miR-146a GFP reporter (Figure 8B), the SASP reporter we have previously generated (Kang et al., 2015). Besides, TNIP1 expression only marginally increased p21 expression and affected neither $p16^{INK4a}$ expression nor 5-bromo-2'-deoxyuridine (BrdU) incorporation (see below, Figure 8C), suggesting that TNIP1 is primarily involved in SASP regulation, not in senescence growth arrest. KEAP1 or UST expression did not affect any of these pathways, indicating that they might modulate senescence-associated phenotypes that are not directly related to senescence growth arrest or the SASP (see below, Figures 8B-D). In addition, TRAF2 expression further increased SASP reporter activity, whereas NFATC4 expression decreased it in senescent cells (Figure 8B). Thus, TRAF2 and NFATC4 might be involved in SASP regulation. Ectopic expression of TRAF2, PEX11B, FLCN, TRAF3, and PARP9 increased BrdU incorporation under normal conditions, suggesting a potential role for them in cell cycle regulation (Figure 8C). As TRAF2 and PEX11B were identified as senescence-regulated autophagy substrates (Figure 6A), their degradation during senescence might contribute to senescence growth arrest. None of our candidates rescued cell cycle arrest in senescent cells when ectopically expressed, indicating the redundant regulation of senescence growth arrest. As NIPSNAP2 did not affect any of the senescence markers we examined, the roles of its autophagic degradation during senescence require further investigation. Together, these results support our hypothesis that autophagy modulates the features of senescence through the selective degradation of its regulatory components. To further examine how this set of selective autophagy functions in the stress support network of senescence, we focused on two potential autophagy substrate proteins, KEAP1 and TNIP1, based on their effects on

senescence markers when ectopically expressed and their reported roles in the stress response (Akbar et al., 2015; Sanchez-Martin and Komatsu, 2020). In addition, we decided to examine a potential role for autophagic degradation of the eIF3 complex in protein homeostasis (proteostasis) during senescence (Hipp et al., 2019; Kaushik and Cuervo, 2015), a multi-protein complex recovered from GO analysis of the SAAI.

Selective Autophagy of KEAP1 Promotes Oxidative Stress Resistance in Senescent Cells

KEAP1 is an adaptor protein for the CUL3 ubiquitin ligase complex that promotes proteasomal degradation of NRF2, a key regulator of the antioxidant defense system. Previous studies showed that p62 either competes with NRF2 for its binding to KEAP1 or causes autophagic degradation of KEAP1, which in turn activates the NRF2 pathway under oxidative stress condition (Bae et al., 2013; Ichimura et al., 2013; Komatsu et al., 2010; Taguchi et al., 2012). We found that the abundance of KEAP1 protein, but not mRNA, decreased during DNA damage-induced and replicative senescence (Figure 9A; Figure 10A). Depletion of the essential autophagy genes ATG7 and ATG13, as well as pharmacological inhibition with the ULK1 inhibitor SBI-0206965, rescued the reduced levels of KEAP1 protein during senescence (Figures 9A and 9B; Figures 10A). Bulk autophagy induced by mTOR inhibition did not affect the abundance of KEAP1 protein (Figure 9C), suggesting a senescence-specific role for autophagy in KEAP1 degradation. Consistently, KEAP1 interaction with p62 increased during senescence (Figure 10B). The phosphorylation of p62 on Ser349, a well-known post-translational modification of p62 that

enhances its binding affinity for KEAP1 (Ichimura et al., 2013), increased in senescent cells (Figure 10C), which might be due to the increased activity of mTOR during senescence (Figure 10D). Furthermore, depletion of p62 rescued the reduced levels of KEAP1 protein in senescent cells but only marginally affected those in normal cells (Figure 10C). Thus, these data suggest that p62 mediates selective autophagy of KEAP1, which in turn might activate the NRF2 pathway during senescence. We confirmed NRF2 pathway activation in senescent cells through gene set enrichment analysis (GSEA) during DNA damage-induced and replicative senescence (Figure 11A-C) (Hernandez-Segura et al., 2017). Furthermore, we verified that several targets of the NRF2 pathway were induced during senescence by reverse transcription qPCR (RT-qPCR; Figure 11A and 11D).

Senescent cells were reported to undergo a complex series of metabolic changes associated with altered mitochondrial activity, which in turn increases oxidative stress (Wiley and Campisi, 2016). Thus, we reasoned that senescent cells require NRF2 pathway activation via autophagy of KEAP1 to tightly maintain their redox homeostasis. If so, senescent cells would be more resistant to oxidative stress than normal cells. Indeed, senescent cells cleared exogenous reactive oxygen species (ROS) significantly faster than normal cells (Figure 12A). Furthermore, DNA damage-induced and replicative senescent cells were more resistant to oxidative stress-induced cell death than normal cells (Figure 12A and 12B). Ectopic expression of KEAP1 suppressed the activation of antioxidant genes downstream of the NRF2 pathway during senescence but did not affect the expression of IL1A (Figure 12C). KEAP1 expression did not affect SA-β-gal activity in senescent cells (Figure 12D), suggesting that its effect on the antioxidant program is not simply due to the suppression of senescence. Consistently, KEAP1

expression partially resensitized senescent cells to oxidative stress (Figure 12E). Together, these data suggest that upon senescence induction, p62-dependent selective autophagy degrades KEAP1, which in turn activates the NRF2 pathway to maintain redox homeostasis in senescent cells and promote their viability.

Selective Autophagy of eIF3 Mitigates Proteotoxic Stress during Senescence

We next considered whether the identification of several eIF3 components in the SAAI might suggest a potential role for their autophagic degradation during senescence (Figure 13A). Indeed, the abundance of several eIF3 subunit proteins, but not their mRNA, decreased during DNA damage-induced and replicative senescence (Figure 9A; Figures 13B and 13C). Several eIF3 subunit proteins were stabilized by inhibition of autophagy during DNA damage-induced and replicative senescence (Figure 13D; Figures 9A and 9B), yet bulk autophagy did not affect the abundance of several eIF3 subunit proteins (Figure 9C). Among the autophagy receptors tested, NDP52 appeared to preferentially bind eIF3 components (Figure 13E). Consistently, NDP52 depletion, but not p62 depletion, partially rescued the reduced levels of several eIF3 subunit proteins during senescence (Figure 10C; Figure 13F). RPS6 and RPL13a, ribosomal proteins, as well as eIF4E, another component of the translation initiation complex, were not subjected to NDP52-dependent selective autophagy during senescence (Figure 13F), indicating that the reduced levels of several eIF3 complex components are unlikely related to ribophagy, selective autophagy of the ribosome. Of note, the abundance of RPS6, RPL13a, and eIF4E proteins decreased during senescence, in part due to their reduced mRNAs (Figure 13F). Together, these data suggest that

autophagy selectively degrades several eIF3 components using NDP52 as a major receptor during senescence.

eIF3 is the largest translation initiation factor composed of 13 different subunits, which is key for translation initiation, termination, and ribosomal recycling (Cate, 2017). Interestingly, the mTOR pathway is activated in senescent cells (Figure 10D), which has been reported to increase the translation of a specific subset of mRNAs and thus support high levels of SASP production (Herranz et al., 2015; Laberge et al., 2015). This could lead to proteotoxic stress observed in senescent cells (Kaushik and Cuervo, 2015). Thus, we hypothesized that autophagy of several eIF3 components might limit the burden of protein synthesis at a certain threshold, maintaining proteostasis during senescence. We found that the global translation rate increased during DNA damage-induced and replicative senescence, and NDP52 depletion further augmented it (Figures 14A and 14B). This could be attributed to the increased number of monosomes and polysomes upon NDP52 depletion in senescent cells through the stabilization of eIF3 components (Figure 14C). Neither p62 depletion nor ATG7 depletion increased the global translation rate in senescent cells (Figure 14D), supporting a specific role for NDP52-dependent autophagy in protein translation during senescence.

Given that senescent cells experience proteotoxic stress, we wondered whether the autophagic restraint of protein translation might have a role in proteostasis during senescence. To investigate this possibility, we took advantage of Proteostat dye, a molecular rotor dye that detects misfolded and aggregated proteins (Shen et al., 2011). Both DNA damage-induced and replicative senescent cells exhibited increased Proteostat staining compared to that in normal cells (Figures 14A and 14B), indicating the accumulation of protein aggregates in senescent cells, as previously reported

(Kaushik and Cuervo, 2015). NDP52 depletion further increased Proteostat staining in senescent cells, but not in normal cells (Figures 14A and 14B), suggesting a context-dependent role of eIF3 autophagic degradation in proteostasis. Notably, inhibition of the proteasome had a similar effect on Proteostat staining in both control and NDP52-depleted senescent cells, indicating that NDP52 depletion was unlikely to exert its effect on protein aggregate formation during senescence by disturbing general proteostasis (Figure 14A). Consistently, NDP52 depletion did not affect overall levels of polyubiquitinated proteins under normal and senescent conditions (Figure 14E). To corroborate these findings, we examined the effect of NDP52 depletion on the long-term survival of senescent cells, their sensitivity to an acute proteotoxic insult, and SASP expression. NDP52 depletion significantly decreased the long-term survival of senescent cells and sensitized senescent cells, but not normal cells, to proteotoxic stress induced by tunicamycin, a well-known ER stressor (Figure 15A), reinforcing a role for selective autophagy of eIF3 components in proteostasis during senescence. NDP52 depletion also partially suppressed the activation of several SASP genes but did not affect the expression of $p16^{INK4a}$ (Figure 15B). Together with recent studies (Herranz et al., 2015; Laberge et al., 2015; Lessard et al., 2018), these data likely reflect a failure to coordinate protein translation to support high levels of SASP production upon NDP52 depletion during senescence. Thus, NDP52-dependent selective autophagy of eIF3 components helps senescent cells to maintain the minimum levels of proteostasis in response to massive protein secretion for the SASP and thus promotes their viability.

Selective Autophagy of TNIP1 Sustains Full Activation of the SASP

Lastly, we explored a possible role for selective autophagy of TNIP1 during senescence. TNIP1 was known to form a functional complex with the deubiquitinase TNFAIP3, which in turn negatively regulates the NF-κB pathway (G'Sell et al., 2015). We identified TNIP1 as a novel interactor of OPTN in the SAAI, and TNIP1 protein abundance decreased during DNA damage-induced and replicative senescence (Figure 9A; Figure 16A). Interestingly, TNIP1 mRNA levels significantly increased during senescence (Figure 16A), suggesting negative feedback loop activation of the NF-κB pathway, as TNIP1 is a known downstream target of NF-κB (G'Sell et al., 2015). Inhibition of autophagy rescued decreased levels of TNIP1 protein during DNA damage-induced and replicative senescence (Figures 9A and 9B; Figures 16A and 16B). Bulk autophagy did not affect the abundance of TNIP1 protein (Figure 9C), suggesting a senescence-specific role for autophagy in TNIP1 degradation. Furthermore, the interaction between TNIP1 and OPTN increased during senescence (Figure 16C). TNIP1 bound OPTN through its N-terminal ABIN homology domain (AHD4), and OPTN bound TNIP1 through its N-terminal NEMO-like domain (Figure 16D). Interestingly, the Ubiquitin Binding domain in ABIN proteins and NEMO domain (UBAN) through which OPTN is known to recognize its targets (e.g., damaged mitochondria) was not necessary for the interaction with TNIP1 (Heo et al., 2015; Richter et al., 2016), suggesting a novel mode of interaction that might involve the intrinsically disordered region (IDR) in the N-terminus of OPTN and TNIP1 (Figure 16E). TNIP1 increased its colocalization with LAMP1, a key component of the lysosome, and OPTN during senescence upon autophagy inhibition (Figures 17A

and 17B). Together, these data suggest that TNIP1 is targeted for selective autophagy during senescence through its association with OPTN.

One unique feature of the SASP is its sustained pattern of activation, which is distinctive from acute inflammation despite the fact that both are mainly regulated by the NF-κB pathway (Chien et al., 2011). The NF-κB pathway is sophisticatedly wired with positive and negative feedback loops to timely manage its activity. Thus, a positive feedback loop of the NF-κB pathway should surpass the negative feedback loop to sustain the SASP. While how the positive feedback loop is activated has been recently reported (De Cecco et al., 2019; Herranz et al., 2015; Laberge et al., 2015), the mechanism disabling the negative feedback loop remains largely unknown. We hypothesized that OPTN-dependent selective autophagy of TNIP1 plays such a role, as TNIP1 is a negative regulator of the NF-κB pathway. Consistently, TNIP1 expression suppressed NF-κB activation as determined by RELA phosphorylation and decreased expression of several SASP genes (Figure 18A). More importantly, depletion of OPTN rescued reduced levels of TNIP1 protein during DNA damage-induced and replicative senescence, which in turn suppressed the activation of NF-κB and several SASP genes (Figures 18B-E). These results suggest a failure to inactivate the negative feedback loop of the NF-κB pathway upon OPTN depletion during senescence. Consistent with this interpretation, depletion of TNIP1 reversed the effect of OPTN depletion on SASP activation (Figures 18D and 18E). Of note, TNIP1 expression has a dichotomous effect on senescence, increasing SA-β-gal activity through activation of the p53–p21 pathway in normal cells, but suppressing the SASP in senescent cells (Figure 8A; Figure 18A). In addition, TNIP1 expression did not affect SA-β-gal activity in senescent cells

(Figure 18F). To further strengthen the importance of TNIP1 degradation in SASP regulation, we examined whether the genetic rescue of TNIP1 affects the paracrine senescence activity of the SASP (Acosta et al., 2013). TNIP1 expression in senescent cells significantly suppressed their paracrine senescence activity (Figure 19). Together, these results suggest that OPTN-dependent selective autophagy of TNIP1 disables a negative regulatory axis of the NF-κB pathway and thus primes senescent cells for full activation of the SASP.

Selective Autophagy Networks during Senescence Appear to be Conserved *in vivo*

To corroborate our finding with *in vivo* human data, we examined the abundance of KEAP1, eIF3 proteins, and TNIP1 in human osteoarthritis (OA) cartilage, a senescence-associated human disease. Senescent chondrocytes accumulated in mouse and human cartilage tissue during OA development. Genetically eliminating senescent cells delayed OA progression and restored the tissue structure in mice (Jeon et al., 2017; Kang et al., 2019). Consistently, the abundance of senescence markers such as $p16^{INK4a}$ and GATA4 increased in the damaged region of human OA cartilage compared to that in the undamaged region. More importantly, we found a significant reduction in the abundance of KEAP1, eIF3 components (eIF3B and eIF3L), and TNIP1 proteins in the damaged region of human OA cartilage relative to that in the undamaged region (Figures 20A and 20B). Chondrocytes expressing a higher level of $p16^{INK4a}$ protein display decreased expression of KEAP1 and eIF3B proteins (Figure 21). In addition, previous transcriptional profiling of human OA cartilage (Ramos et al., 2014) indicated that KEAP1, eIF3B, and TNIP1 are not

regulated at the mRNA level in human OA (Figure 22A). Collectively, these data suggest that the abundance of KEAP1, eIF3 components, and TNIP1 proteins are reduced at the post-transcriptional level during *in vivo* senescence with human OA progression, echoing our cellular findings that they are regulated by autophagy during senescence. To further verify these results, we performed GSEA analysis on transcriptional profiling of human OA cartilage (Ramos et al., 2014). We confirmed NRF2 and SASP pathway activation signatures during human OA progression, which presumably resulted from selective autophagy of KEAP1 and TNIP1, respectively (Figure 22B). Thus, selective autophagy might contribute to senescence and its associated phenotypes during human OA progression.

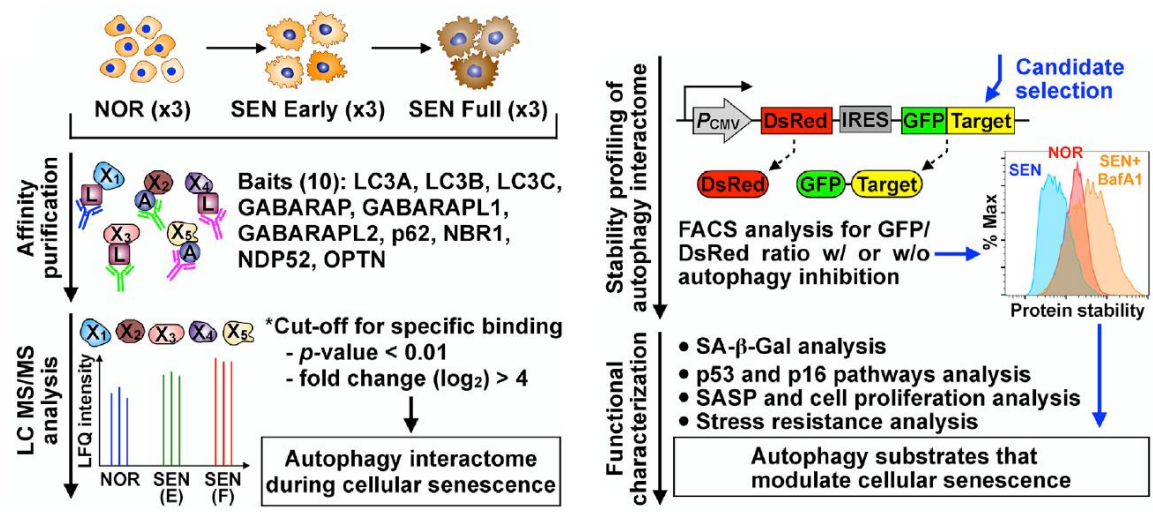

Figure 1. Schematic representation of selective autophagy substrates identification platform during senescence.

To systematically discover autophagy substrate proteins, proteomics screen was proceeded to identify proteins showing alterations in their interaction with the ATG8 family proteins and several autophagy receptors during senescence and candidate proteins were selected, referred as the senescence-associated autophagy interactome (SAAI). To identify autophagy substrate proteins in the SAAI, a focused genetic screening using the Global Protein Stability (GPS) system was proceeded to search for a protein for which stability was changed in an autophagy-dependent manner during senescence. Next, functional characterization was proceeded for SAAI proteins by examining multiple senescence markers including senescence-associated-β-galactosidase (SA-β-Gal) activity, cell cycle arrest, and the activation of three main branches of the senescence regulatory network, namely the p53-p21, $p16^{INK4a}$, and SASP pathways.

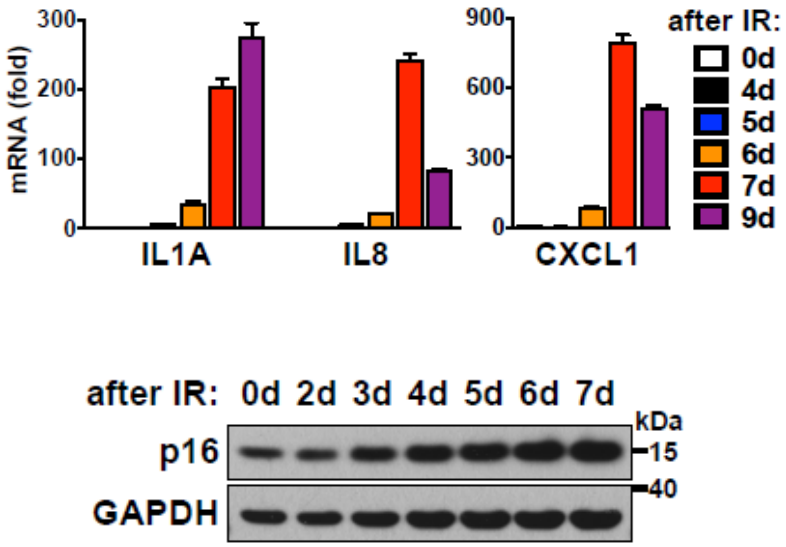

Figure 2. Expression of SASP and $p16^{INK4a}$ changes during senescence

Abundance of the indicated mRNAs during IR-induced senescence was analyzed by RT-qPCR (top, mean ± error). Immunoblotting showing abundance of p16 protein during IR-induced senescence (bottom).

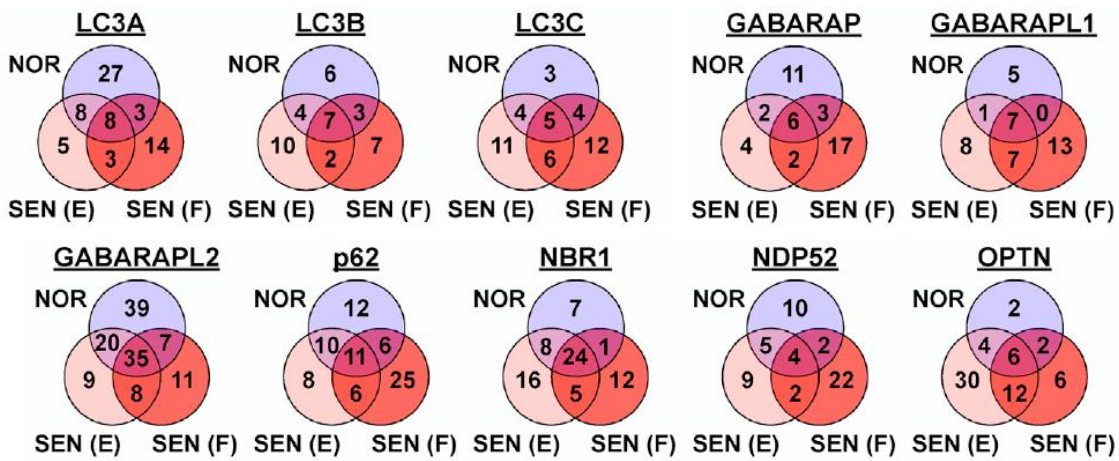

Figure 3. Venn diagrams summarizing autophagy interactome during cellular senescence

Proteins that interact with the indicated ATG8 family of proteins or autophagy receptors across each stage of senescence were identified. A total of 360 non-redundant proteins making 634 interactions in the SAAI were identified (68 for LC3A, 39 for LC3B, 45 for LC3C, 45 for GABARAP, 41 for GABARAPL1, 129 for GABARAPL2, 78 for p62, 73 for NBR1, 54 for NDP52, and 62 for OPTN)

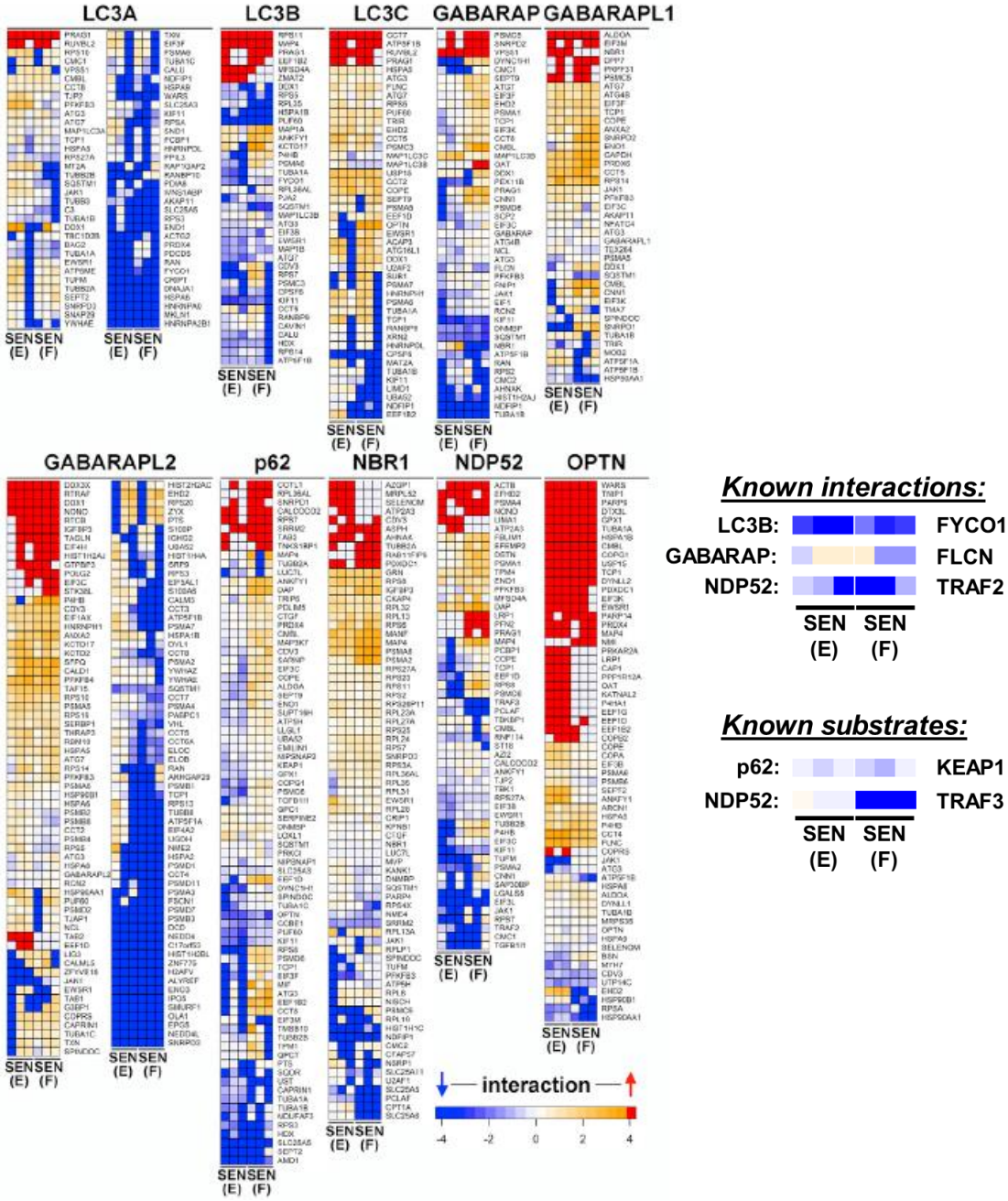
LC3A
LC3B
LC3C
GABARAP
GABARAPL1
GABARAPL2
p62
NBR1
NDP52
OPTN
SEN SEN
(E) (F)
interaction
-4
-2
0
2
4
Known interactions:
LC3B:
FYCO1
GABARAP:
FLCN
NDP52:
TRAF2
SEN SEN
(E) (F)
Known substrates:
p62:
KEAP1
NDP52:
TRAF3
SEN SEN
(E) (F)

Figure 4. Heatmap representation of senescence-associated autophagy interactome (SAAI)

Changes in binding affinity with ATG8 family proteins or autophagy receptors were analyzed. Increased interactions in early senescence [SEN (E)] or in fully senescent cells [SEN (F)] compared to normal control cells (NOR) are colored red and decreased interactions compared to NOR are colored blue. The SAAI revealed previously known interactions such as LC3B–FYCO, GABARAP-FLCN and NDP52–TRAF2, as well as recently identified autophagy substrate proteins such as KEAP1 and TRAF3

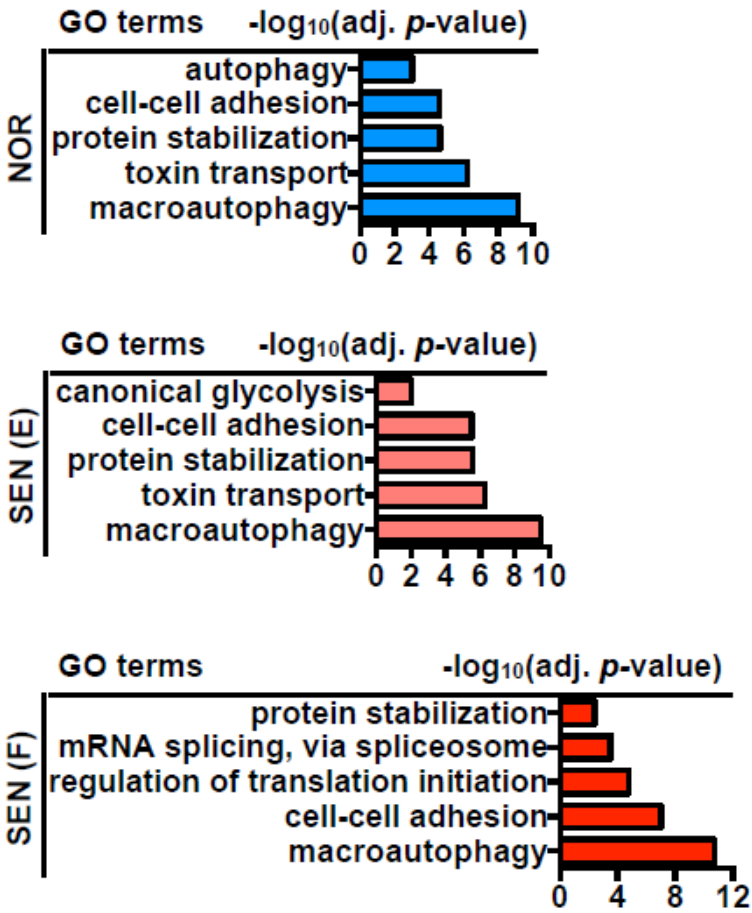

Figure 5. GO term analysis of the SAAI proteins

Gene ontology (GO) analysis of the SAAI showed significant enrichment in biological processes related to autophagy regardless of the stage of senescence. The term "canonical glycolysis" was enriched in early senescence. The terms "mRNA splicing, via spliceosome" and "regulation of translation initiation" were enriched in full senescence.

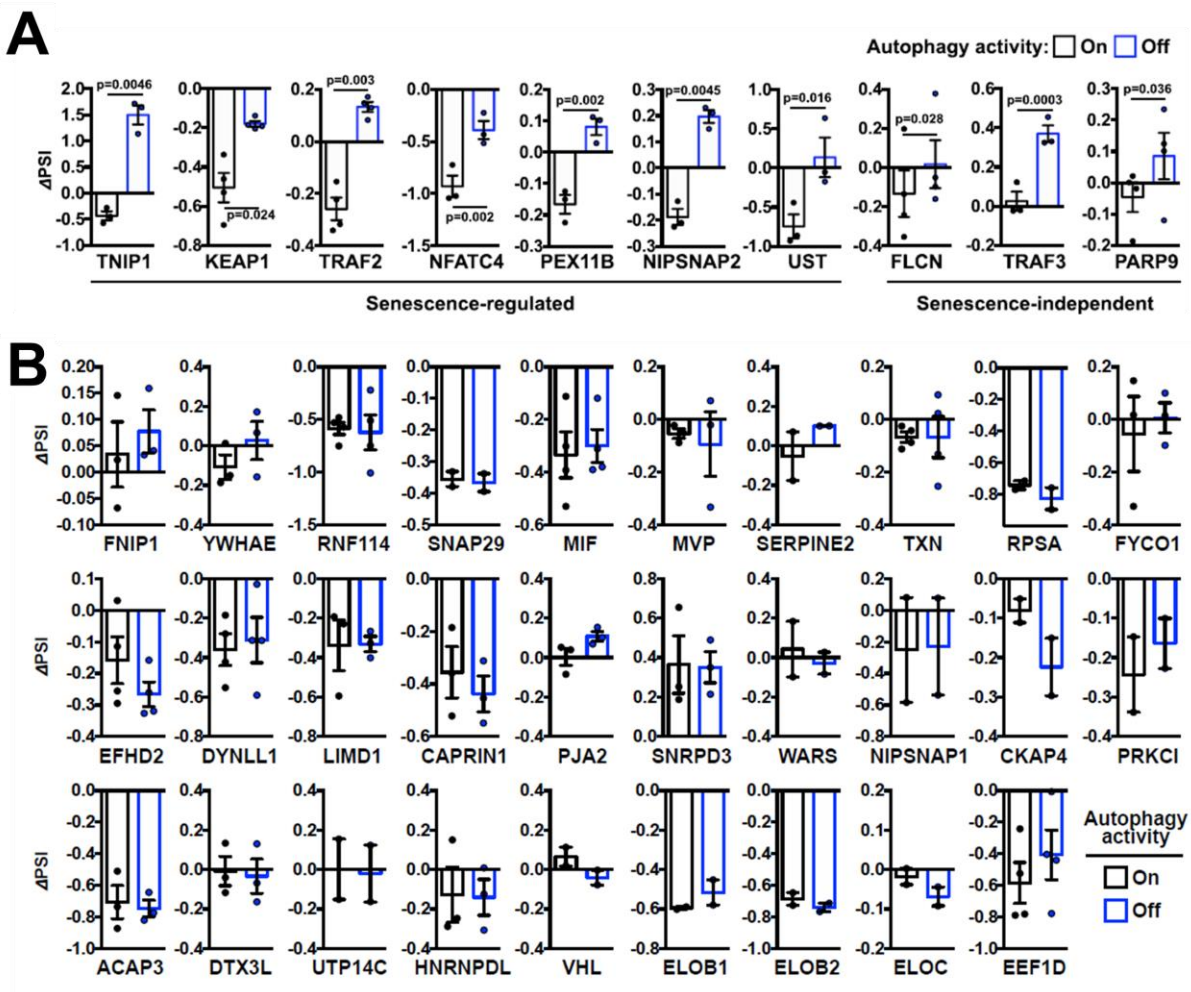

Figure 6. Determination of protein stability of 39 SAAI proteins using the GPS system.

Relative changes in protein stability index (PSI) were measured by FACS (mean ± SEM, paired t test). Of the 39 examined proteins, the stability of 17 proteins significantly decreased during senescence.

(A) Inhibition of autophagy increased the stability of 10 proteins (class I SAAI proteins).

(B) Protein stability of 29 SAAI proteins. Relative changes in protein stability index (PSI) were measured (mean ± SEM, n = 3 except for RNF114, MIF, TXN, EFHD2, DYNLL1, and EEF1D, where n = 4, and SNAP29, SERPINE2, RPSA, WARS, NIPSNAP1, CAKP4, PRKCI, UTP14C, VHL, ELOB1, ELOB2, and ELOC, where n = 2, paired t−test).

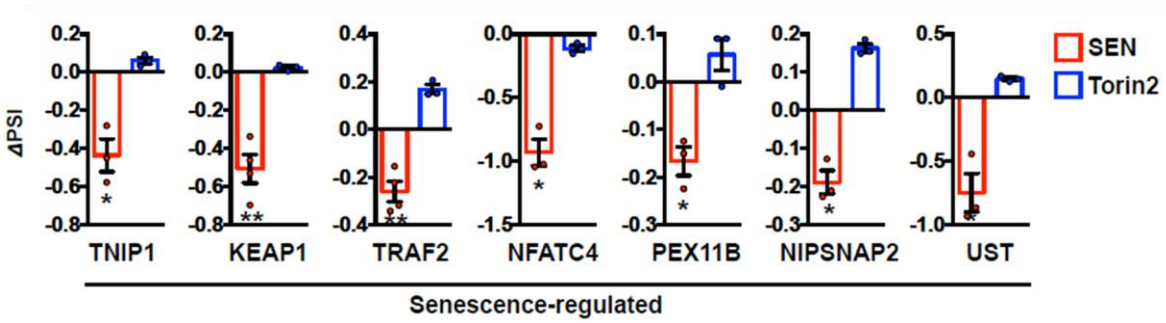

Figure 7. Determination of protein stability of class I SAAI proteins upon the induction of bulk autophagy

Bulk autophagy is not responsible for the reduced protein stability of senescence-regulated class I SAAI proteins. The cells were treated with Torin 2 (100 nM) for 12 h to induce bulk autophagy before determining protein stability of senescence- regulated class I SAAI proteins using the GPS system. Relative changes in protein stability index (PSI) were measured as in Figure 6 (mean ± SEM, *p<0.05, **p<0.01, one-sample t-test).

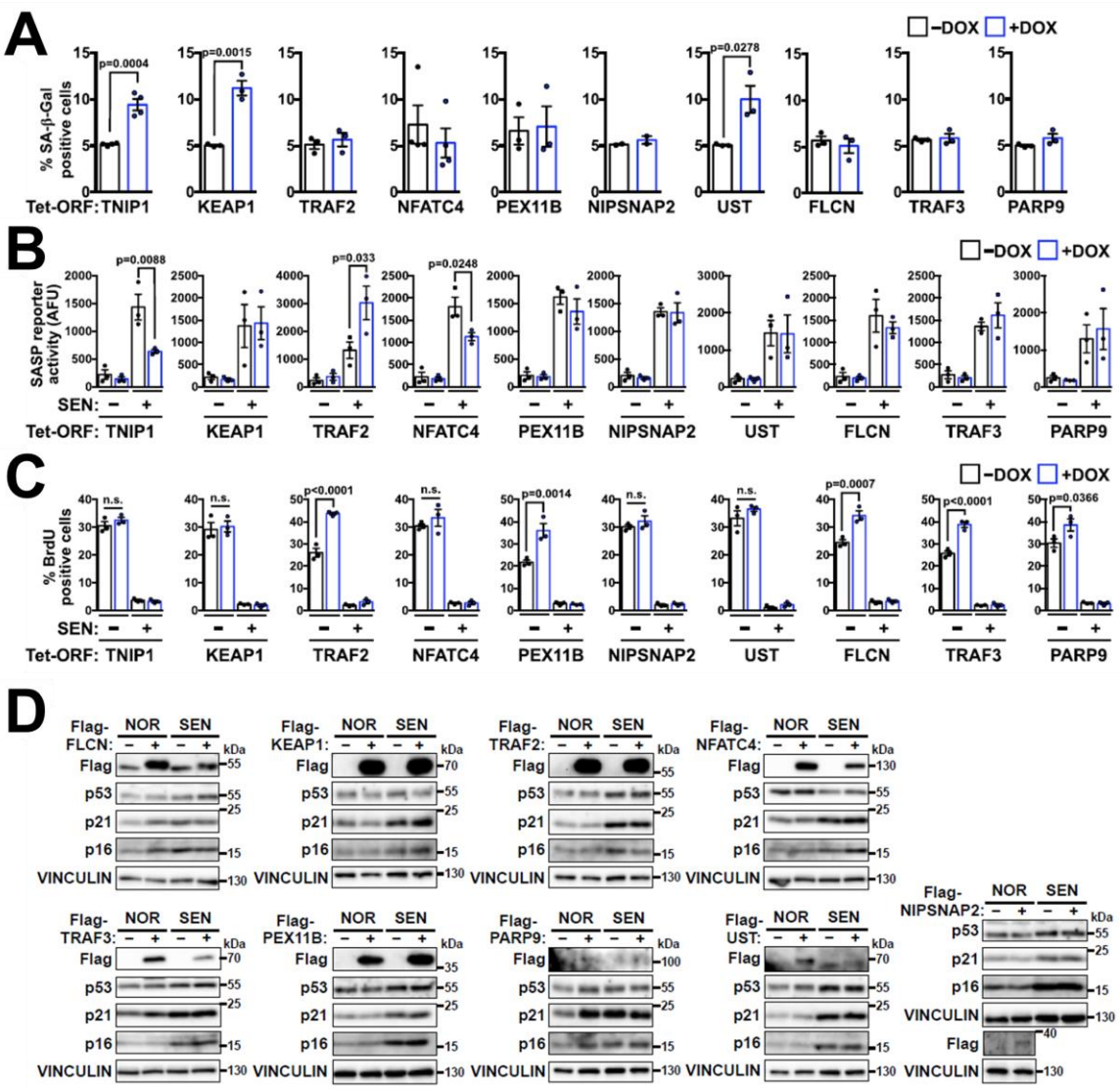
A
−DOX +DOX
% SA-β-Gal positive cells
p=0.0004
p=0.0015
p=0.0278
Tet-ORF: TNIP1 KEAP1 TRAF2 NFATC4 PEX11B NIPSNAP2 UST FLCN TRAF3 PARP9
B
SASP reporter activity (AFU)
p=0.0088
p=0.033
p=0.0248
SEN: − +
C
% BrdU positive cells
n.s.
p<0.0001
p=0.0014
p=0.0007
p=0.0366
D
Flag-FLCN: NOR SEN
Flag-KEAP1: NOR SEN
Flag-TRAF2: NOR SEN
Flag-NFATC4: NOR SEN
Flag-TRAF3: NOR SEN
Flag-PEX11B: NOR SEN
Flag-PARP9: NOR SEN
Flag-UST: NOR SEN
Flag-NIPSNAP2: NOR SEN
Flag
p53
p21
p16
VINCULIN
kDa

Figure 8. Functional characterization of Class I SAAI proteins in the senescence regulatory network

(A) Quantification of the percentage of SA-β-gal positive cells (mean ± SEM, unpaired t-test).

(B) Quantification of the miR-146a GFP reporter activity (mean ± SEM, two-way ANOVA test). AFU denotes arbitrary fluorescence units.

(C) Quantification of BrdU incorporation (mean ± SEM, one-way ANOVA test).

(D) IMR90 cells carrying a Dox-inducible vector expressing the indicated class I SAAI genes were grown with or without Dox, treated with bleomycin to induce senescence, and immunoblotting was performed (n = 2).

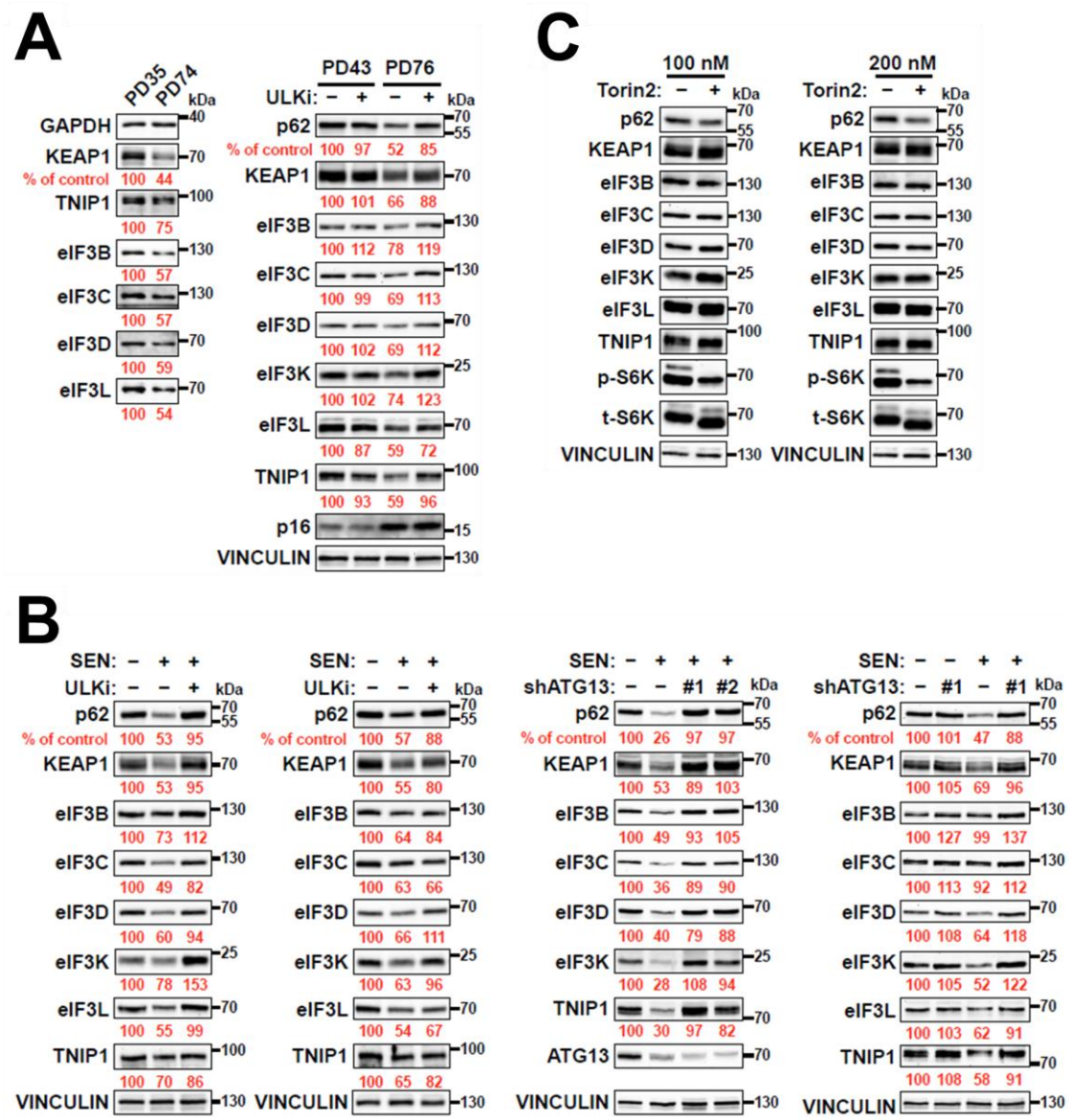
A
PD35
PD74
kDa
GAPDH
40
KEAP1
70
% of control 100 44
TNIP1
100
100 75
eIF3B
130
100 57
eIF3C
130
100 57
eIF3D
70
100 59
eIF3L
70
100 54
PD43 PD76
ULKi: − + − + kDa
p62
70
55
% of control 100 97 52 85
KEAP1
70
100 101 66 88
eIF3B
130
100 112 78 119
eIF3C
130
100 99 69 113
eIF3D
70
100 102 69 112
eIF3K
25
100 102 74 123
eIF3L
70
100 87 59 72
TNIP1
100
100 93 59 96
p16
15
VINCULIN
130
C
100 nM
200 nM
Torin2: − + kDa
p62
70
55
KEAP1
70
eIF3B
130
eIF3C
130
eIF3D
70
eIF3K
25
eIF3L
70
TNIP1
100
p-S6K
70
t-S6K
70
VINCULIN
130
B
SEN: − + +
ULKi: − − + kDa
p62
70
55
% of control 100 53 95
KEAP1
70
100 53 95
eIF3B
130
100 73 112
eIF3C
130
100 49 82
eIF3D
70
100 60 94
eIF3K
25
100 78 153
eIF3L
70
100 55 99
TNIP1
100
100 70 86
VINCULIN
130
SEN: − + +
ULKi: − − + kDa
p62
70
55
% of control 100 57 88
KEAP1
70
100 55 80
eIF3B
130
100 64 84
eIF3C
130
100 63 66
eIF3D
70
100 66 111
eIF3K
25
100 63 96
eIF3L
70
100 54 67
TNIP1
100
100 65 82
VINCULIN
130
SEN: − + + +
shATG13: − − #1 #2 kDa
p62
70
55
% of control 100 26 97 97
KEAP1
70
100 53 89 103
eIF3B
130
100 49 93 105
eIF3C
130
100 36 89 90
eIF3D
70
100 40 79 88
eIF3K
25
100 28 108 94
TNIP1
70
100 30 97 82
ATG13
70
VINCULIN
130
SEN: − − + +
shATG13: − #1 − #1 kDa
p62
70
55
% of control 100 101 47 88
KEAP1
70
100 105 69 96
eIF3B
130
100 127 99 137
eIF3C
130
100 113 92 112
eIF3D
70
100 108 64 118
eIF3K
25
100 105 52 122
eIF3L
70
100 103 62 91
TNIP1
70
100 108 58 91
VINCULIN
130

Figure 9. Autophagy selectively targets KEAP1, eIF3 complex components, and TNIP1 for degradation in senescence

(A) Abundance of the indicated proteins was analyzed during replicative senescence (left, n = 3). Inhibition of ULK1 rescued the reduced levels of KEAP1, eIF3 complex components, and TNIP1 during replicative senescence. The cells were treated with SBI-0206965 (10 μM) for 24 h before sampling to block autophagy.

(B) Inhibition of ULK1 rescued the reduced levels of KEAP1, eIF3 complex components, and TNIP1 during senescence. The cells were treated with SBI-0206965 (10 μM) before sampling to block autophagy (left). Knockdown of ATG13 rescued the reduced levels of KEAP1, eIF3 complex components, and TNIP1 during senescence (right).

(C) Bulk autophagy is not responsible for the reduced levels of KEAP1, eIF3 complex components, and TNIP1 during senescence. The cells were treated with Torin 2 for 6 h to induce bulk autophagy. Immunoblotting analysis was performed for the indicated proteins (n = 3).

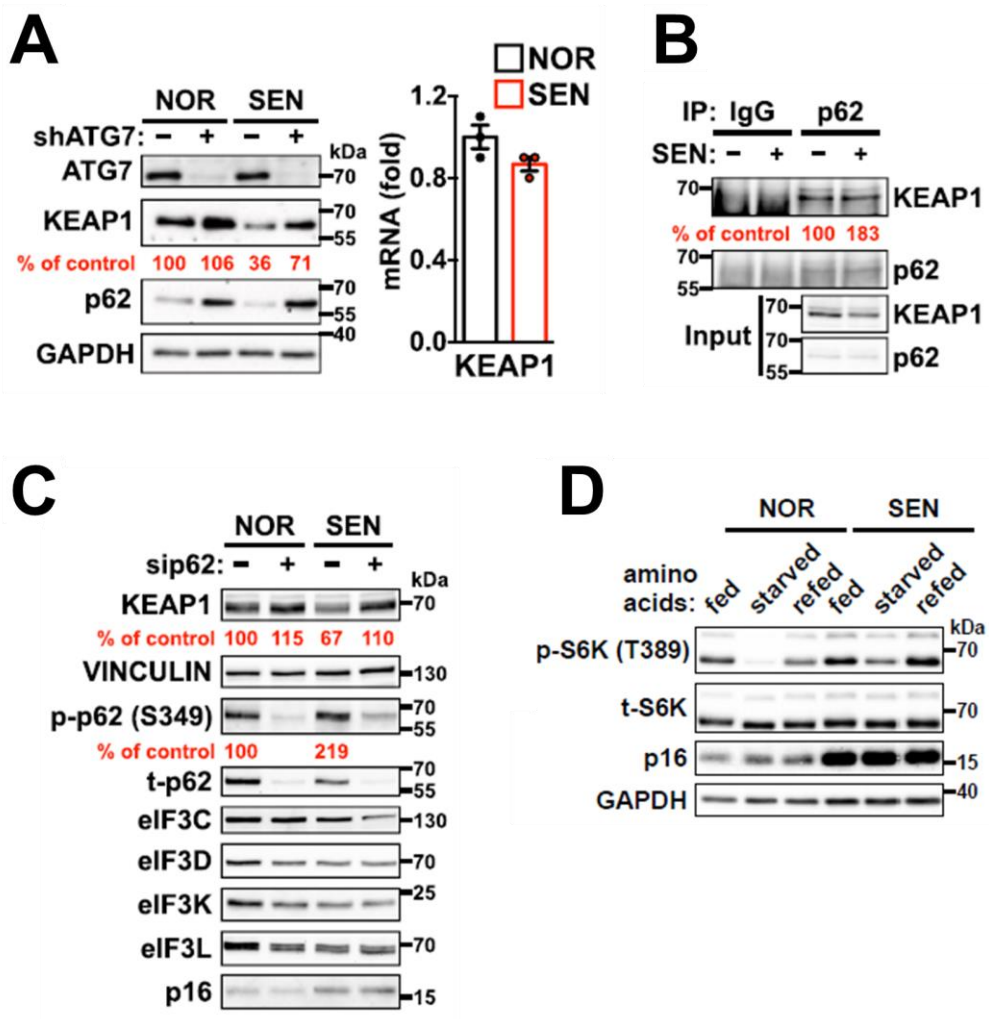

Figure 10. KEAP1 is a target of p62−mediated selective autophagy in senescence

(A) Abundance of the indicated proteins analyzed by immunoblotting (left). Abundance of KEAP1 mRNA analyzed by RT−qPCR (right, n = 3, mean ± SEM).

(B) Immunoblotting of endogenous p62 immunoprecipitates. The immunoprecipitate signals were normalized to input levels.

(C) Abundance of the indicated proteins analyzed by immunoblotting. Immunoblotting signals for the phospho−p62 were normalized to total p62 levels. n = 2.
(D) The mTOR pathway is activated in senescent cells. The cells were starved for amino acids for 3 h followed by amino acid refeeding (10 m) before sampling. Immunoblotting analysis was performed for the indicated proteins (right, n = 3).

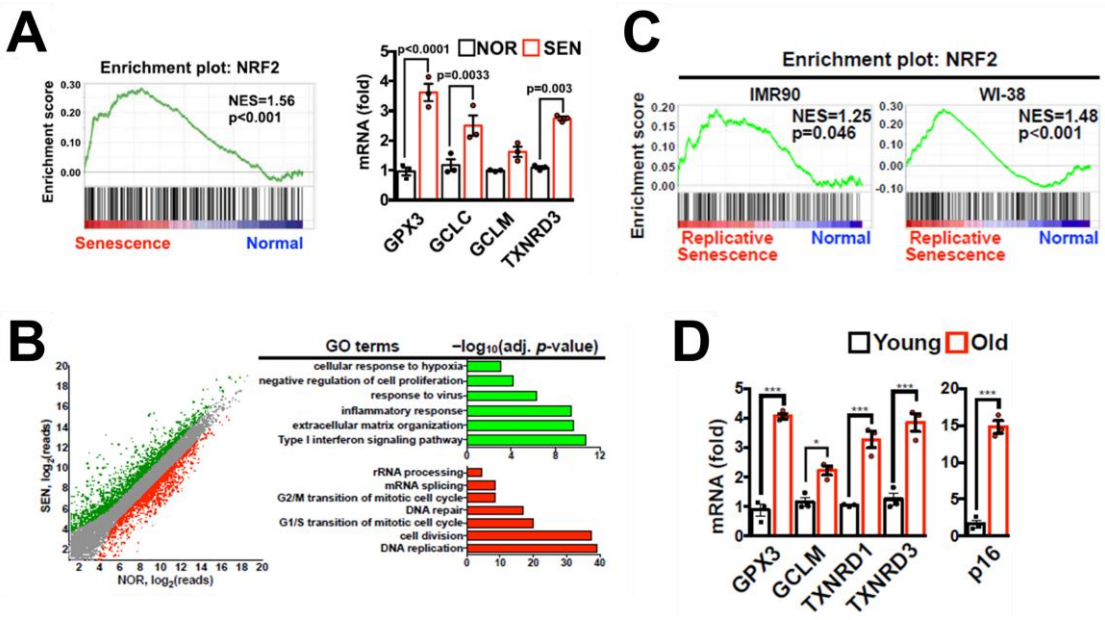

Figure 11. NRF2 pathway is activated in senescence

(A) GSEA of differentially expressed genes during DNA damage-induced senescence (left). NES denotes normalized enrichment score. Abundance of the indicated mRNAs analyzed by RT-qPCR (right, mean ± SEM, n = 3, one-way ANOVA test).

(B) mRNA expression profiling from normal and bleomycin-induced senescent IMR90 cells identified genes that were significantly up-regulated (green, more than 200% expression of normal, Q < 0.05) or down-regulated (red, less than 50% expression of normal, Q < 0.05) upon senescence induction (left). GO term analysis of the up-regulated (green) or down-regulated (red) genes (right).

(C) Gene set enrichment analysis of DEGs in replicative senescent IMR90 cells (left) and WI-38 cells (right) of the NRF2 pathway. NES denotes normalized enrichment score.

(D) Abundance of mRNAs for the indicated genes was quantified by RT-qPCR during replicative senescence (right, mean ± SEM, n = 3, *p<0.05, **p<0.01, ***p<0.001, one-way ANOVA test). Young and Old denote PD 40~41 and PD 84~85 IMR90 cells, respectively.

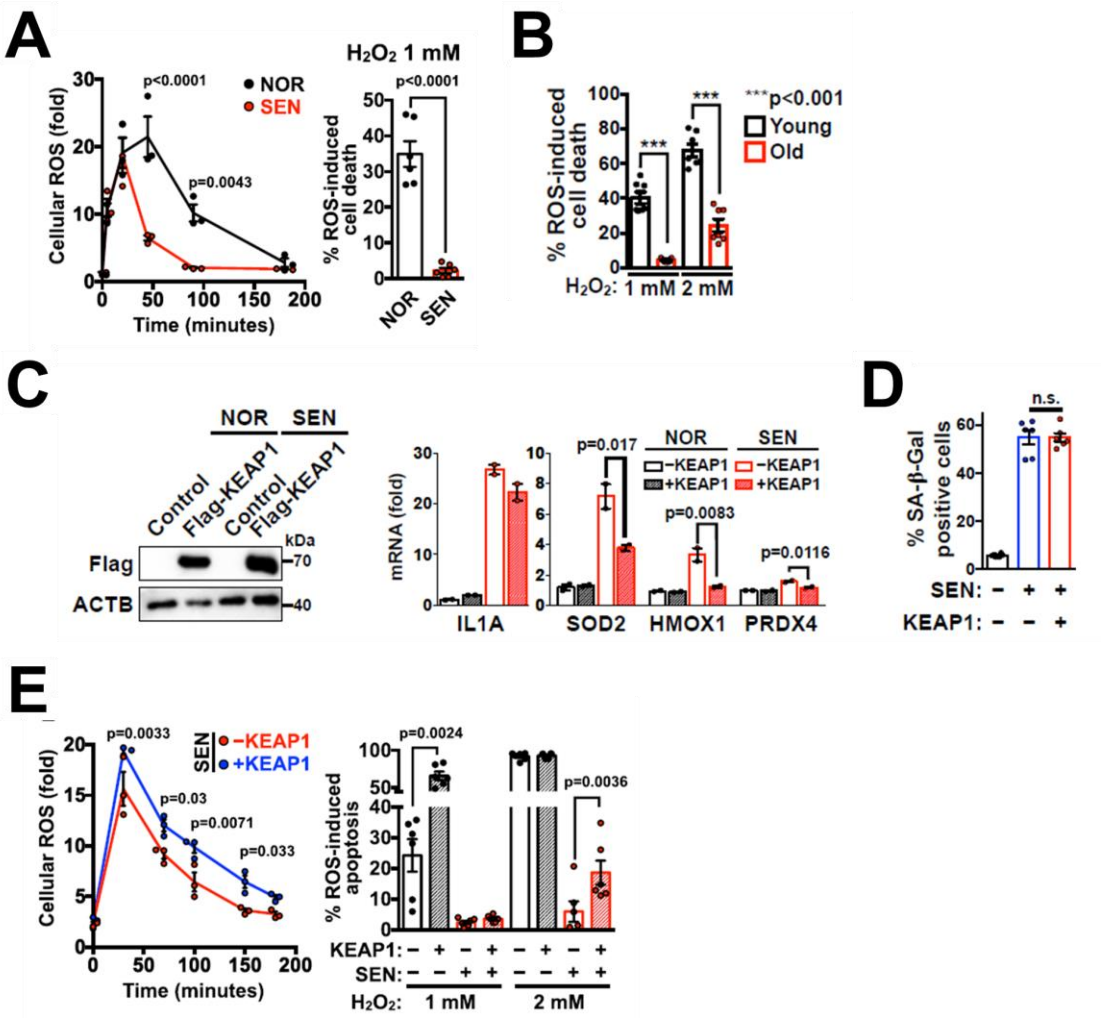

Figure 12. Selective autophagy of KEAP1 activates the NRF2 pathway and promotes oxidative stress resistance

(A) ROS decay analysis (left, normalized mean ± SEM, n = 4, two-way ANOVA test). ROS-induced cell death analyzed by the propidium iodide (PI) uptake assay (right, normalized mean ± SEM, n = 6, unpaired t-test).

(B) Young (PD = 35~40) and old (PD = 74~78) IMR90 cells were challenged with 1 mM or 2 mM H_2O_2 for 24 h and cell death was

determined by FACS using the propidium iodide (PI) uptake assay (normalized mean ± SEM, n = 7, one-way ANOVA test).
(C) IMR90 cells carrying a vector expressing KEAP1 or an empty vector were treated with bleomycin to induce senescence. Abundance of proteins was analyzed by Western blotting (left). Abundance of mRNAs for the indicated genes was quantified by RT-qPCR (right, n = 2, mean ± SEM, one-way ANOVA test).
(D) SA-β-Gal staining in IMR90 cells carrying a Dox-inducible (Tet-On) vector expressing KEAP1 was analyzed by FACS (mean ± SEM, n = 6, one-way ANOVA test).
(E) ROS decay analysis (left, normalized mean ± SEM, n = 3, two-way ANOVA test). ROS-induced apoptosis analyzed by a FITC annexin V apoptosis detection kit (right, normalized mean ± SEM, n = 6, one-way ANOVA test).

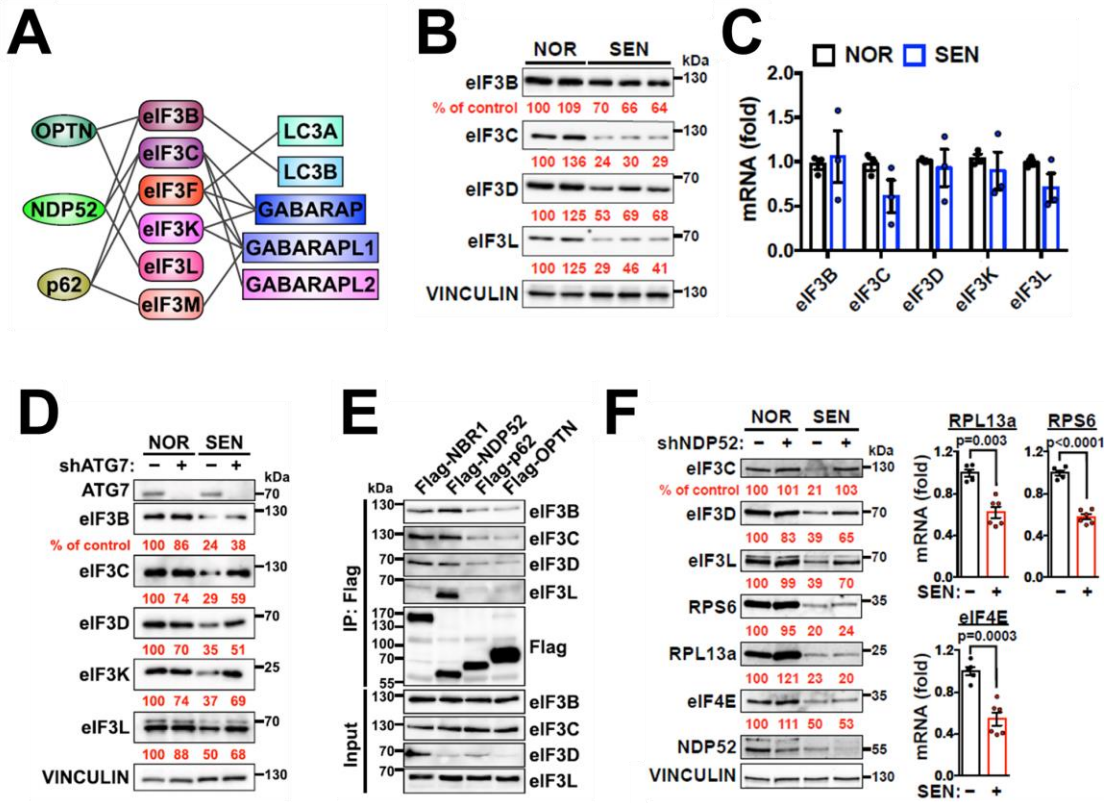

Figure 13. eIF3 complex is a target of NDP52-mediated selective autophagy in senescence

(A) Schematic representation of eIF3 interaction network from the SAAI.

(B) IMR90 cells were treated with bleomycin to induce senescence, and immunoblotting analysis was performed.

(C) RT-qPCR analysis of the abundance of the indicated mRNAs during bleomycin-induced senescence (n = 3, mean ± SEM).

(D) Abundance of the indicated proteins analyzed by immunoblotting (n = 3).

(E) Immunoblotting of Flag immunoprecipitates (n = 2).

(F) NDP52 depletion did not affect the levels of RPS6, RPL13a, and

eIF4E proteins during senescence. Immunoblotting analysis was performed for the indicated proteins (n = 2, left). Abundance of mRNAs for the indicated genes was quantified by RT−qPCR during senescence (right, mean ± SEM, n = 6, unpaired t−test).

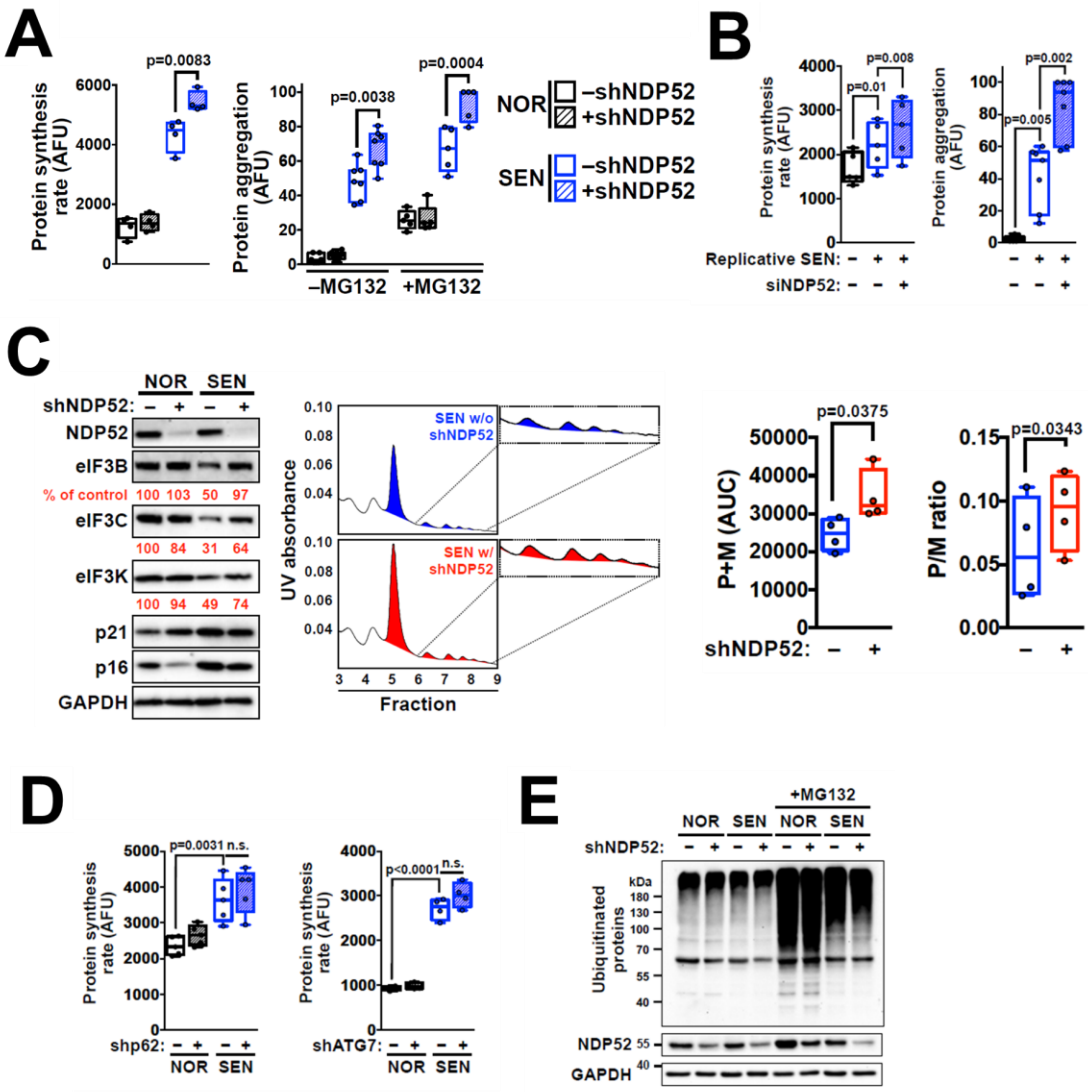

Figure 14. Selective autophagy of eIF3 limits protein translation and maintains proteostasis during senescence

(A) Quantification of global protein synthesis rate (left, box plots show the 1st and 3rd quartiles; whiskers show the minimum and maximum values, n = 4, one-way ANOVA test) and protein aggregation (right, box plots show the 1st and 3rd quartiles; whiskers show the minimum and maximum values, n = 7 for without MG-132 and n = 5 with MG-132, two-way ANOVA test).

(B) NDP52 depletion increased the global protein synthesis (left, box plots show the 1st and 3rd quartiles; whiskers show the minimum and maximum values, n = 5, one-way ANOVA test) and protein aggregates (right, box plots show the 1st and 3rd quartiles; whiskers show the minimum and maximum values, n = 7, one-way ANOVA test) during replicative senescence. Replicative SEN denotes PD 84~85 IMR90 cells.

(C) IMR90 cells carrying a vector expressing an NDP52 shRNA were treated with bleomycin to induce senescence, and immunoblotting analysis was performed (left). Representative polysome profiling (center), sum of polysome and monosome areas (P+M), polysome-to-monosome (P/M) ratio (right, box plots show the 1st and 3rd quartiles; whiskers show the minimum and maximum values, n = 4, paired two-tailed t-test). The higher P+M and P/M ratio, the higher global translation rate.

(D) Neither p62 depletion nor ATG7 depletion affected the global protein synthesis during senescence [box plots show the 1st and 3rd quartiles; whiskers show the minimum and maximum values, n = 5 for p62 depletion (left), n = 4 for ATG7 depletion (right), one-way ANOVA test]

(E) NDP52 depletion did not affect the levels of poly-ubiquitinated proteins during senescence. The cells were treated with MG132 (50 μM for 6 h) Immunoblotting analysis was performed for the indicated proteins (n = 3). Poly-ubiquitinated proteins were detected by anti-ubiquitinylated proteins antibody (clone FK2).

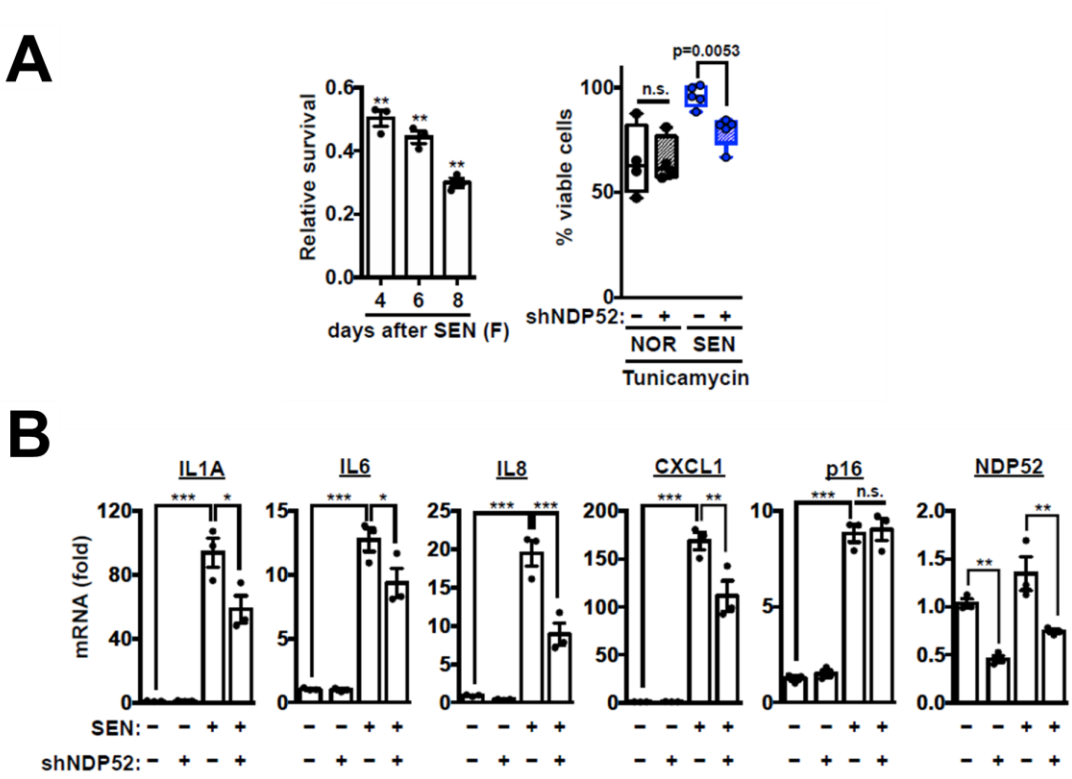

Figure 15. Selective autophagy of eIF3 support senescent cell from proteotoxic stress for cell viability and SASP

(A) NDP52 depletion decreased the long-term survival of senescent cells. The relative survival rate was analyzed by FACS at the indicated day after full senescence establishment (7 days after 12Gy IR) (left, n = 3, **p < 0.01, one-sample t-test). NDP52 depletion sensitized senescent cells to proteotoxic stress induced by tunicamycin (10 mg/ml, 18 h). Cell death was determined FACS using a FITC annexin V apoptosis detection kit (right, box plots show the 1st and 3rd quartiles; whiskers show the minimum and maximum values, multiple t-test with correction for multiple comparisons).

(B) NDP52 depletion partially suppressed expression of several SASP genes during senescence. Abundance of mRNAs for the indicated genes was quantified by RT-qPCR (n = 3, mean ± SEM, *p < 0.05, **p < 0.01, ***p < 0.001, one-way ANOVA test).

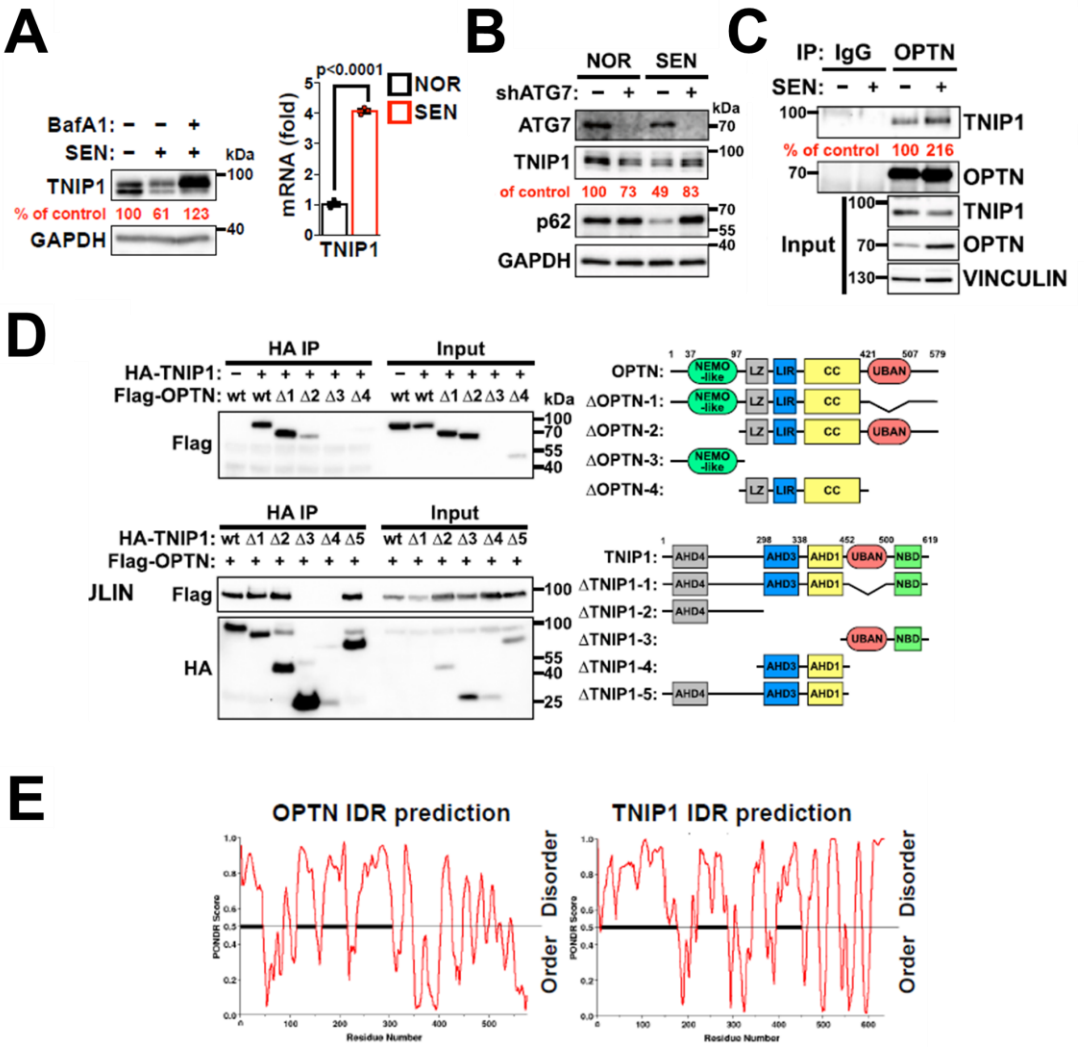

Figure 16. TNIP1 is a target of OPTN-mediated selective autophagy in senescence

(A) Immunoblotting showing abundance of TNIP1 protein during senescence (left). RT-qPCR analysis of the abundance of TNIP1 mRNA during senescence (center, n = 3, mean ± SEM, unpaired two-tailed t-test). Flag-immunoprecipitates were analyzed by

immunoblotting during bleomycin-induced senescence. The immunoprecipitate signals were normalized to input levels (right).
(B) Abundance of the indicated proteins analyzed by immunoblotting.
(C) Immunoblotting of endogenous OPTN immunoprecipitates. The immunoprecipitate signals were normalized to input levels. n = 2.
(D) HEK-293T cells were transfected with a vector expressing HA-tagged OPTN in combination with a vector expressing a series of Flag-tagged OPTN deletion mutants, and HA immunoprecipitates were analyzed by immunoblotting (top left). Of note, ΔOPTN-3 was failed to be expressed, probably due to its low stability. Schematic representation of Flag-tagged OPTN deletion mutants (top right). HEK-293T cells were transfected with a vector expressing Flag-OPTN in combination with a vector expressing a series of HA-tagged TNIP1 deletion mutants, and HA immunoprecipitates were analyzed by immunoblotting (bottom left). Schematic representation of HA-tagged TNIP1 deletion mutants (bottom right). n = 3.
(E) Intrinsically disordered regions in OPTN and TNIP1 were analyzed using the PONDR (Predictor of Natural Disordered Regions, VLXT).

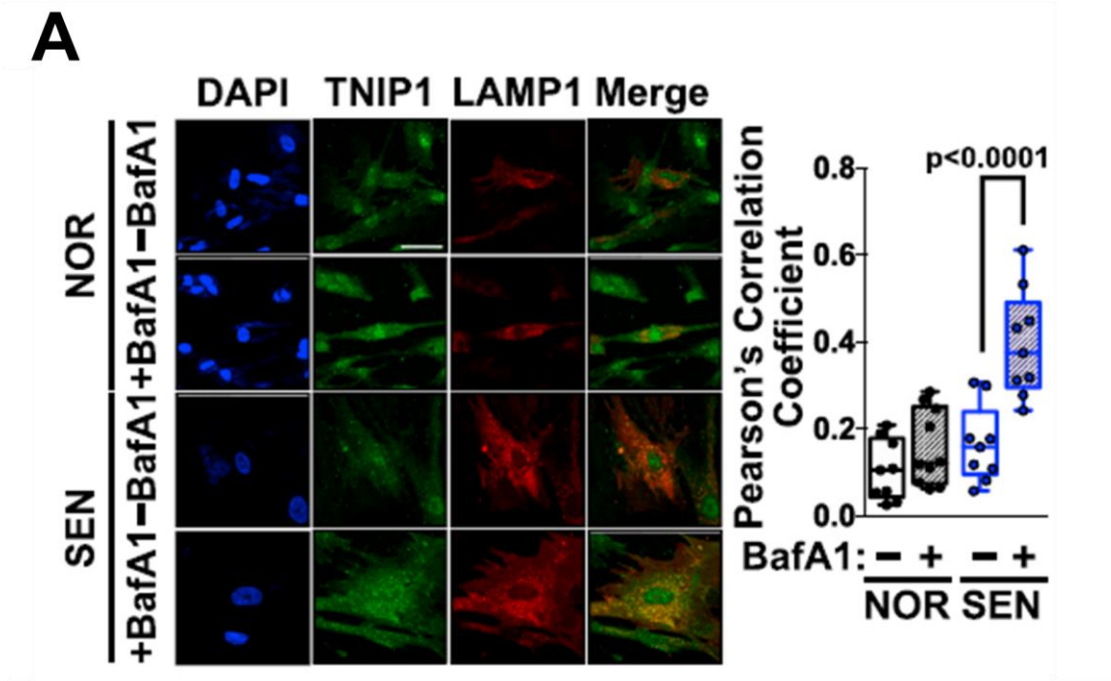
A
DAPI
TNIP1
LAMP1
Merge
NOR
SEN
−BafA1
+BafA1
−BafA1
+BafA1
Pearson's Correlation Coefficient
p<0.0001
0.8
0.6
0.4
0.2
0.0
BafA1: − + − +
NOR SEN

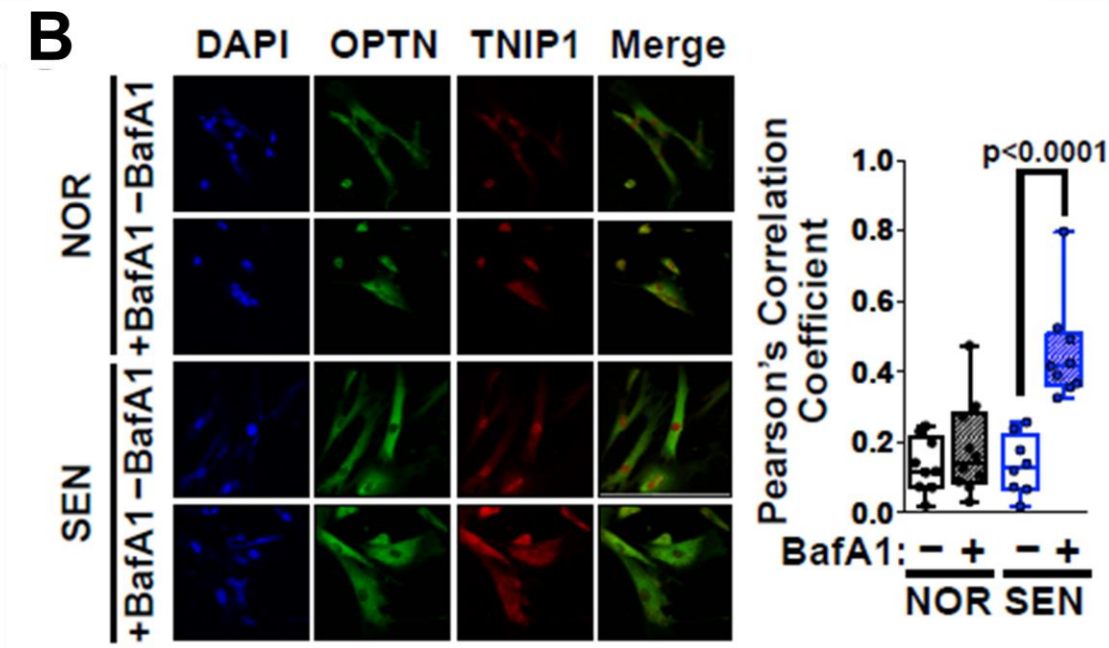
B
DAPI
OPTN
TNIP1
Merge
NOR
SEN
−BafA1
+BafA1
−BafA1
+BafA1
Pearson's Correlation Coefficient
p<0.0001
1.0
0.8
0.6
0.4
0.2
0.0
BafA1: − + − +
NOR SEN

Figure 17. TNIP1 colocalizes with lysosome and OPTN

(A) Immunocytochemistry of the indicated proteins (left). Pearson's correlation coefficient for co-localization of TNIP1 and LAMP1 (right, box plots show the 1st and 3rd quartiles; whisker show the minimum and maximum values, one-way ANOVA test). Scale bar = 50 μm.

(B) Immunocytochemistry of the indicated proteins in normal and senescent IMR90 cells. Pearson's correlation coefficient for co-localization of TNIP1 and OPTN (right, box plots show the 1st and 3rd quartiles; whisker show the minimum and maximum values, one-way ANOVA test).

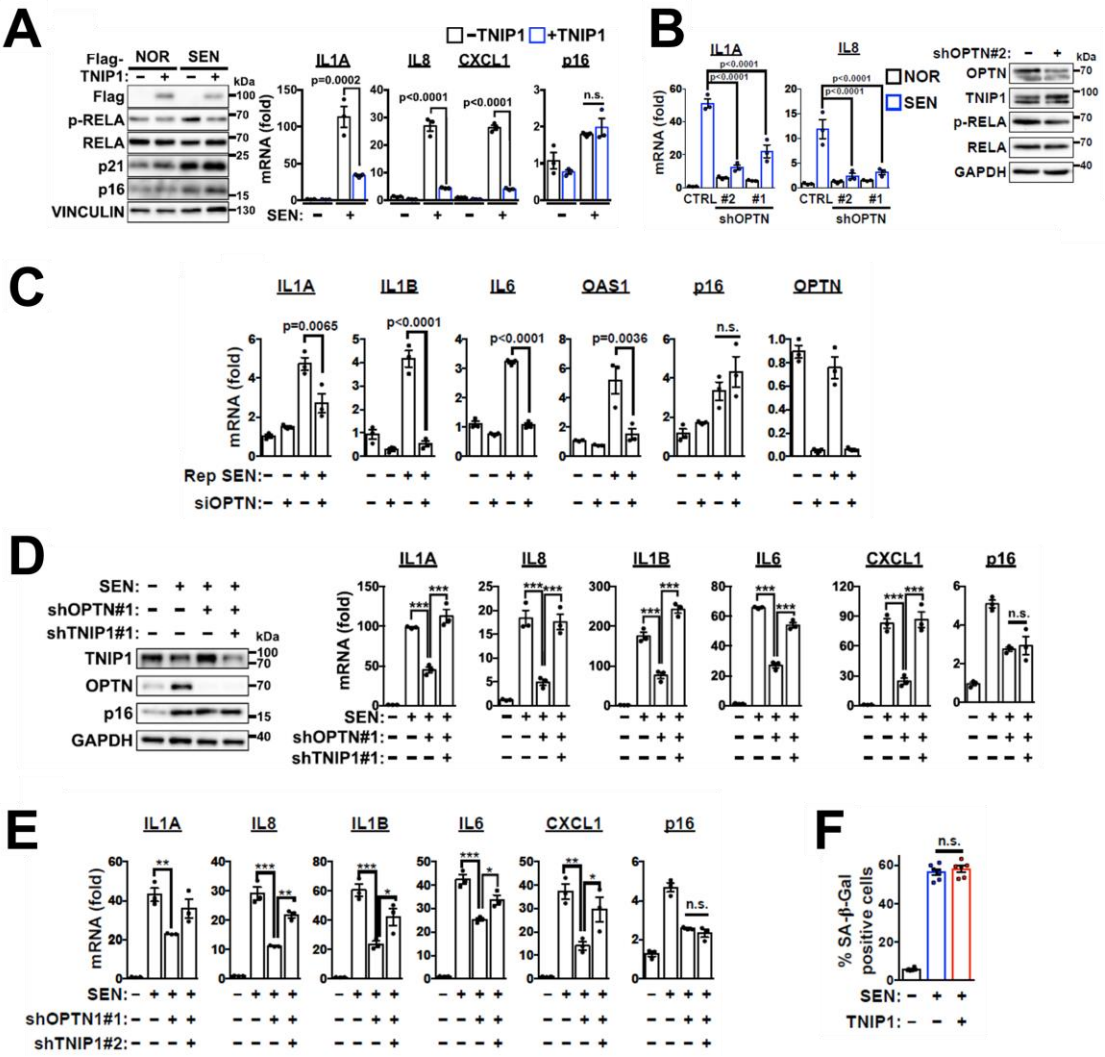

Figure 18. Selective autophagy of TNIP1 enhances senescence-associated inflammation during senescence

(A) Abundance of the indicated proteins analyzed by immunoblotting (left). Abundance of the indicated mRNAs analyzed by RT-qPCR (right, n = 3, mean ± SEM, two-way ANOVA test). (B) IMR90 cells carrying a Dox-inducible vector expressing OPTN shRNAs were treated with bleomycin to induce senescence, grown

with or without Dox, and abundance of mRNAs for the indicated genes was quantified by RT−qPCR (left, n = 3, one−way ANOVA test). Immunoblotting analysis was performed (right, n = 3).

(C) OPTN depletion suppressed full activation of the SASP during replicative senescence. Abundance of mRNAs for the indicated genes was quantified by RT−qPCR (n = 3, mean ± SEM, one−way ANOVA test, Rep SEN denotes PD84~85 IMR90 cells).

(D) Abundance of the indicated proteins analyzed by immunoblotting (left). Abundance of the indicated mRNAs analyzed by RT−qPCR (right, n = 3, mean ± SEM, one−way ANOVA test).

(E) IMR90 cells carrying a Dox−inducible vector expressing a TNIP1 shRNA in combination with a vector expressing an OPTN shRNA were treated with bleomycin to induce senescence, grown with or without Dox. Abundance of mRNAs for the indicated genes was quantified by RT−qPCR (mean ± SEM, n = 3, $*p < 0.05$, $**p < 0.01$, $***p < 0.001$, one−way ANOVA test).

(F) SA−β−Gal staining in IMR90 cells carrying a Dox−inducible (Tet−On) vector expressing TNIP1 was analyzed by FACS (mean ± SEM, n = 6, one−way ANOVA test).

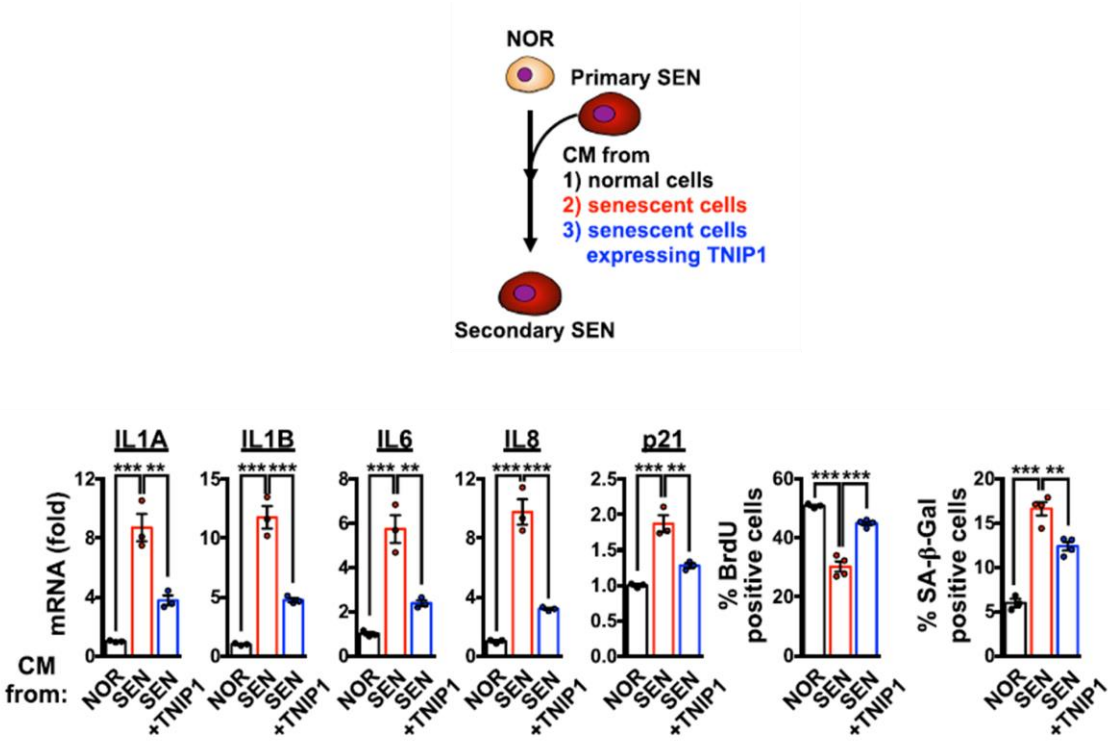

Figure 19. Selective autophagy of TNIP1 primes the paracrine senescence activity of senescent cells

Diagram explaining the CM experiments (top). Abundance of the indicated mRNAs analyzed by RT−qPCR (bottom left, n = 3, mean ± SEM, one−way ANOVA test). BrdU incorporation and SA−β−Gal staining (bottom right, n = 4 except for NOR, where n = 3, mean ± SEM, one−way ANOVA test) were analyzed.

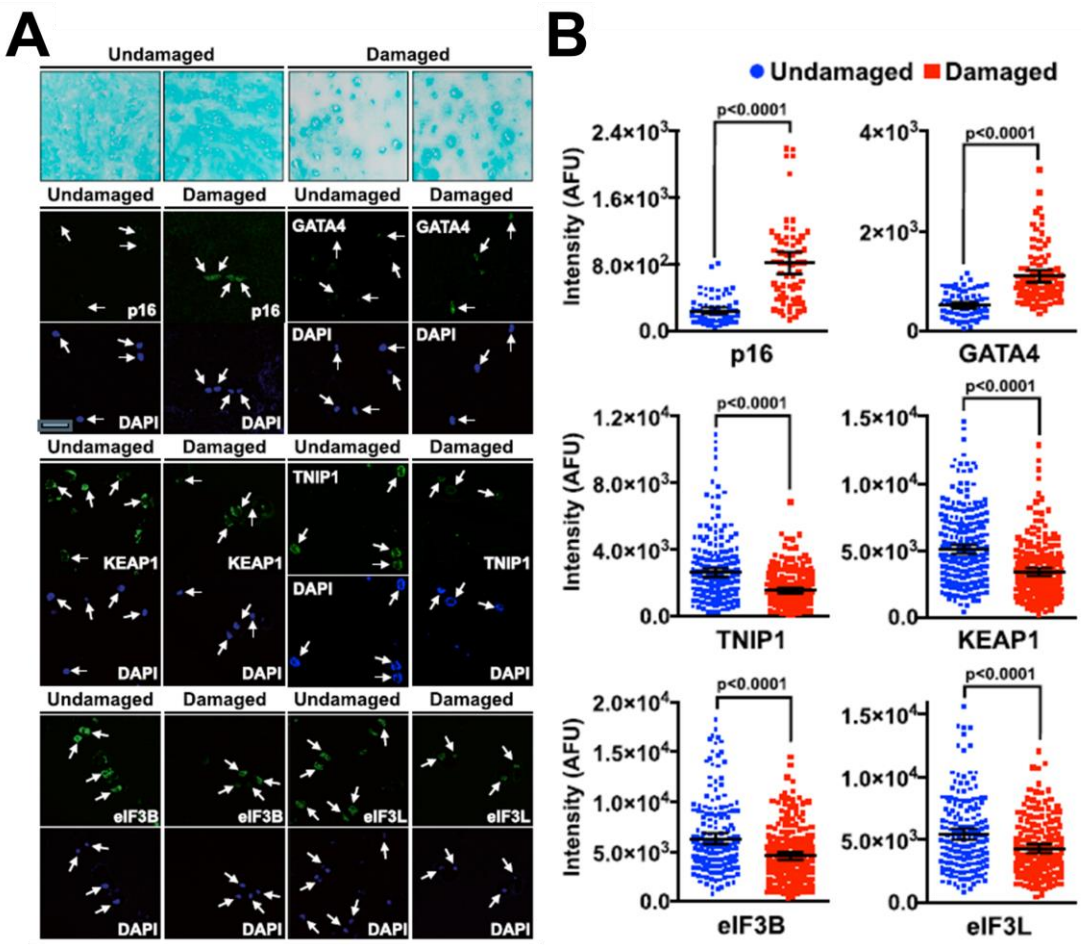

Figure 20. KEAP1, eIF3, TNIP1 expression decreases during human osteoarthritis progression

(A) Alcian blue staining (top) and confocal immunofluorescence labeling for the indicated proteins (bottom) in the cartilage sections from the representative undamaged or damaged region of human OA cartilage. Scale bar = 25 μm.

(B) Quantitative analysis of immunofluorescence of the indicated proteins. Each point represents an individual cell from a total of seven patients (p16, n = 68 for undamaged, n = 61 for damaged;

GATA4, n = 77 for undamaged, n = 85 for damaged; KEAP1, n = 253 for undamaged, n = 214 for damaged; TNIP1, n = 222 for undamaged, n = 210 for damaged; eIF3B, n = 182 for undamaged, n = 207 for damaged; eIF3L, n = 173 for undamaged, n = 173 for damaged. ***$p<0.0001$, unpaired t-test)

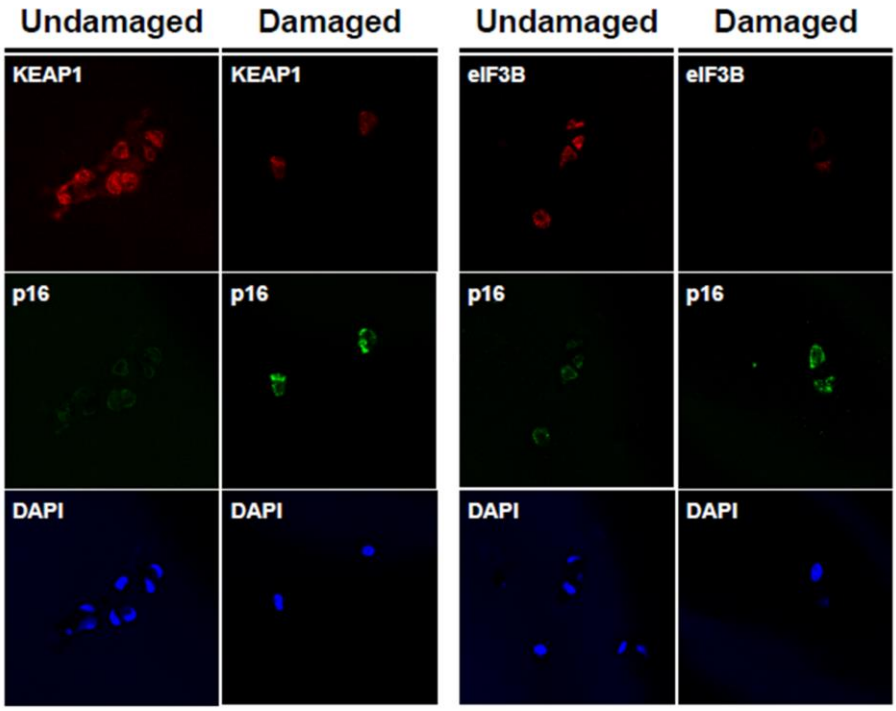
Undamaged
Damaged
Undamaged
Damaged
KEAP1
KEAP1
eIF3B
eIF3B
p16
p16
p16
p16
DAPI
DAPI
DAPI
DAPI

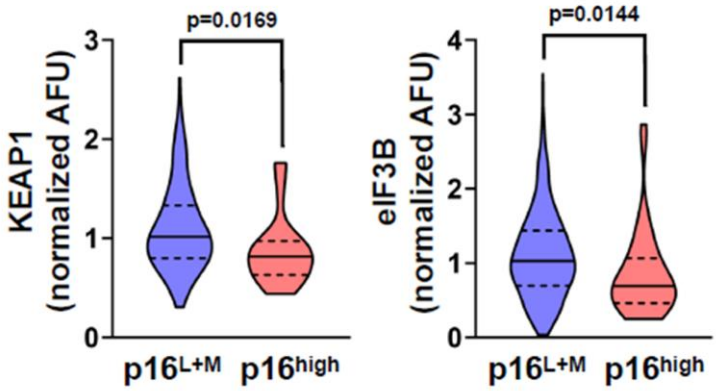
p=0.0169
KEAP1
(normalized AFU)
0
1
2
3
p16L+M
p16high
p=0.0144
eIF3B
(normalized AFU)
0
1
2
3
4
p16L+M
p16high

Figure 21. Chondrocytes expressing a higher level of $p16^{INK4a}$ protein display decreased expression of KEAP1 and eIF3B proteins

KEAP1 and eIF3B expression decreases in p16-positive chondrocytes during Human OA progression. Co-immunofluorescence labeling for the indicated proteins in the cartilage sections from the representative undamaged and damaged region of human OA cartilage (top). Violin plot analysis comparing the abundance of KEAP1 and eIF3B proteins between $p16^{L+M}$ and $p16^{high}$ cells (bottom, the horizontal solid line shows the medium and the horizontal dot lines show the 1st and 3rd quartiles, unpaired t-test). Cells were categorized into 2 groups [$p16^{high}$ (top 20%) and $p16^{L+M}$ (bottom 80%)] according to p16 fluorescence intensity.

A

Transcriptional profiling of human OA cartilage		
Gene	Log_2 (fold)	*p*-value
KEAP1	0.00176	0.973
eIF3B	0.02807	0.691
TNIP1	0.04224	0.370

B

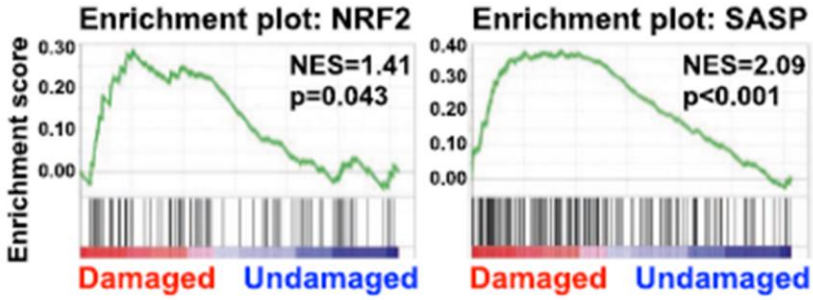

Figure 22. KEAP1, eIF3 components, and TNIP1 proteins are regulated at the post-transcriptional level during in vivo senescence with human OA progression

(A) Transcriptional changes of the indicated genes from transcriptional profiling of human OA cartilage (Ramos et al., 2014)

(B) GSEA of differentially expressed genes in human OA for the NRF2 pathway (left) and the SASP pathway (right).

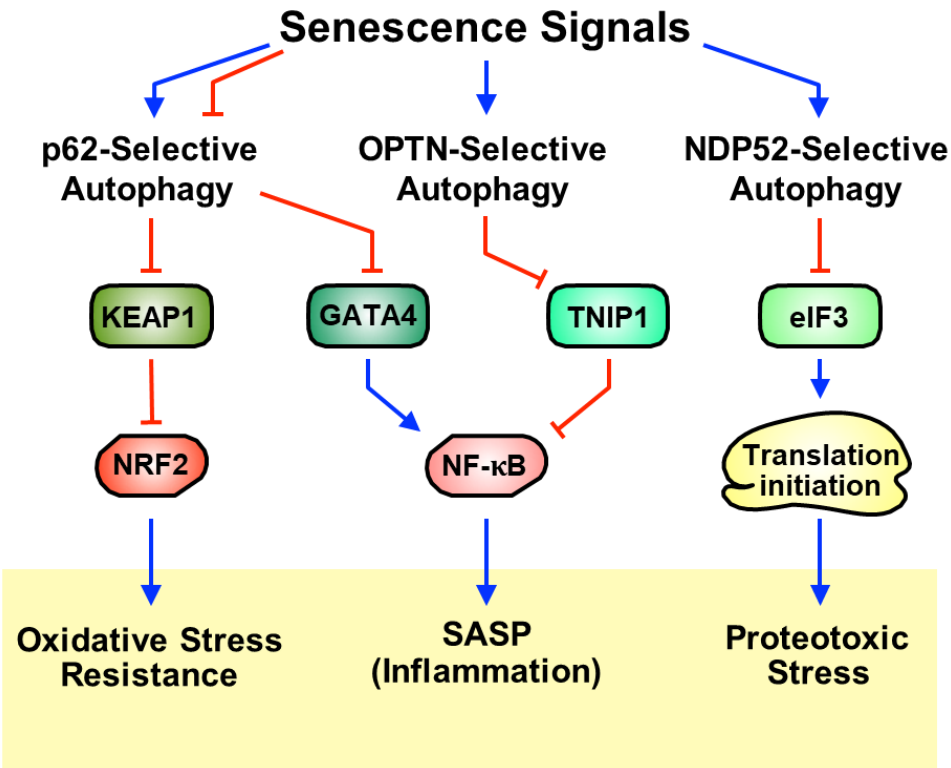

Figure 23. Model of How Selective Autophagy Coordinates the Homeostatic State of Senescence Through Regulated Protein Stability

Our integrated platform provides a comprehensive set of autophagy substrate proteins involved in various senescence-associated processes. By dissecting their roles in senescence, we have demonstrated that selective autophagy contributes to redox homeostasis, proteostasis, and full activation of the SASP in senescent cells. This contribution is achieved through the degradation of KEAP1, several components of the eIF3 complex, and TNIP1.

DISCUSSION

Unraveling the intricate relationship between two critical age-related processes, senescence and autophagy, requires the identification of senescence regulatory components targeted by autophagy at the systems level. Our integrated platform described here represents a significant advance toward this goal by providing a comprehensive set of autophagy substrate proteins involved in various senescence-associated processes. By dissecting their roles in senescence, we have demonstrated that selective autophagy contributes to redox homeostasis, proteostasis, and full activation of the SASP in senescent cells. This contribution is achieved through the degradation of KEAP1, several components of the eIF3 complex, and TNIP1. Thus, our findings greatly enhance our understanding of how autophagy promotes and maintains the senescent state by coordinating the stress support network in senescent cells through the degradation of multiple regulatory components (Figure 23).

Regulation of protein stability is a key mechanism in a wide range of stress responses. While the ubiquitin-proteasome system (UPS) has been extensively studied in this regard, including its role in senescence (exemplified by UPS-dependent regulation of p53 for senescence growth arrest) (Kastenhuber and Lowe, 2017; Pohl and Dikic, 2019)., recent evidence has highlighted the potential of selective autophagy to modulate important cellular processes by targeting regulatory components (Kang and Elledge, 2016; Sánchez-Martín and Komatsu, 2020).. However, the full exploration of autophagy's potential has been hampered by the lack of versatile systems to systematically identify autophagy substrate proteins. Our integrative approach provides a foundation for

exploring this emerging functional module of autophagy. By further investigating the mechanistic details of other autophagy substrates identified in our study, we can gain a better understanding of selective autophagy networks during senescence, which may rival the UPS in importance for controlling senescence through regulated protein stability.

Autophagy is generally considered an anti-senescence mechanism due to its role in cellular quality control and its association with lifespan-promoting interventions (Mizushima and Komatsu, 2011; Pohl and Dikic, 2019). Inhibition of autophagy has been shown to induce senescence in several in vitro and in vivo models under normal conditions (García-Prat et al., 2016; Gewirtz, 2013). However, autophagy is activated upon senescence induction and its impairment paradoxically delays full senescence (Young et al., 2009), suggesting pro-senescence mechanisms of autophagy. Autophagy has been shown to metabolically support senescent cells by exhibiting a massive secretory phenotype, similar to its role in supporting cancer cells (Narita et al., 2011). In addition, autophagy contributes to the degradation of cytoplasmic chromatin fragments associated with nuclear lamina components, thereby reducing DNA damage and promoting senescence (Dou et al., 2015; Ivanov et al., 2013).. Furthermore, recent studies have shown that autophagy promotes senescence by degrading SIRT1, an NAD+-dependent deacetylase (Xu et al., 2020).. Taken together, these findings underscore the context-dependent role of autophagy and the need for a nuanced understanding of when, how, and why autophagy acts in senescence. Our study not only highlights emerging functions of autophagy, but also provides insights into the cellular mechanisms of senescence regulation by autophagy.

Interestingly, autophagy has also been found to play a dual role in tumorigenesis, although most studies of its pro-tumorigenic

activity have focused on metabolic adaptation in cancer cells (Levine and Kroemer, 2019; White, 2015). It is possible that autophagy promotes tumorigenesis by modulating the stress support network in cancer cells through regulated protein stability, similar to the mechanisms identified in senescent cells. For example, the p62-KEAP1-NRF2 axis has been implicated in cancer as an enhancer of stress resistance (Ichimura and Komatsu, 2018). Thus, our systematic approach provides a powerful framework for future studies aimed at discovering novel autophagy substrate proteins involved in tumorigenesis. Identification of such proteins could provide opportunities to develop therapeutic strategies based on non-oncogene addiction, targeting the homeostatic state of cancer cells (Luo et al., 2009). Conversely, strategies used in cancer treatment could potentially be applied to senescence treatment, opening a new chapter in non-senescent senotherapy.

Senescence has recently emerged as a fundamental aging mechanism, and the accumulation of senescent cells is known to promote chronic inflammation through the SASP, thereby contributing to age-related diseases. Limiting the detrimental effects of senescence, such as by eliminating senescent cells or modulating the SASP (senotherapy), holds great promise for the treatment of aging (Childs et al., 2017; Kang, 2019; Kirkland and Tchkonia, 2017; van Deursen, 2019). Therefore, understanding the vulnerability of senescent cells and the regulation of SASP is critical for human health. Our study shows that selective autophagy regulates two critical cytoprotective responses, redox homeostasis and proteostasis, in senescent cells while maintaining high levels of SASP. Exploring the molecular switch that activates selective autophagy upon senescence induction represents an exciting avenue for future research, as tailored modulation of this switch may expand the repertoire of senotherapy options.

The following important questions can be divided into two parts. First, we need to understand the molecular switch responsible for the activation of selective autophagy during senescence. Post-translational modifications such as ubiquitination and phosphorylation, as well as liquid-liquid phase separation (LLPS), are likely to play a critical role in this process (Li, Jingxian, et al., 2022). For example, our research has shown that phosphorylation of SQSTM1 at S349 increases during senescence, thereby increasing its affinity for ubiquitinated substrates. It would be interesting to explore the signaling pathway responsible for this regulation, and the MTOR pathway, which is known to maintain activity during senescence and phosphorylate SQSTM1, is a potential candidate (Ichimura et al., 2013). In addition, ATM/ATR, a DNA damage response (DDR) kinase activated during senescence, may modulate these post-translational modifications. Previous studies have shown that the ATM/ATR signaling pathway regulates the GATA4-SASP pathway (Kang et al., 2015), and since the phosphorylation consensus site for ATM/ATR is conserved in GATA4, it would be interesting to investigate upstream regulators that activate the molecular switch of selective autophagy in senescence. Furthermore, in the case of OPTN-TNIP1 interaction, we have observed that the intrinsically disordered regions of OPTN and TNIP1 are critical. Recent evidence suggests that LLPS, driven by weak multivalent interactions through intrinsically disordered regions, plays a role in the autophagy of multiple substrates (Noda, et al., 2020). Therefore, it would be valuable to investigate whether LLPS is involved in the selective autophagy of TNIP1. Currently, the autophagic regulation of the EIF3 complex and its dependence on NDP62 are not well understood. Since only a subset of EIF3 subunits has been identified in SAAI (Senescence-Associated Autophagy Inhibitor), it is possible that autophagy targets only

specific EIF3 proteins. Identifying the post-translational modification specific to each component or investigating their susceptibility to LLPS may help unravel the mode of autophagic regulation of the EIF3 complex.

The second part of our inquiry involves understanding the roles of autophagic regulation in the remaining substrate proteins identified in our study. Notably, we discovered multiple components of spliceosomes and metabolic pathways in the SAAI. Given that senescent cells exhibit alternative splicing events and rewiring of metabolic pathways, it would be fascinating to investigate to what extent selective autophagy contributes to these remodeling processes during senescence. Such exploration could reveal additional therapeutic targets for senotherapy. Furthermore, among the class I SAAI proteins, senescence-independent autophagy substrates are also of interest. For instance, the FLCN-FNIP tumor suppressor complex is sequestrated by GABARAP-conjugated membrane compartments. This suggests that FLCN-FNIP regulates cytosolic RagC-GTP and that its sequestration on intracellular membranes restricts access to this substrate, resulting in nuclear retention of TFEB/TFE3 due to impaired Rag binding. This TFEB activation pathway is permissive with mTORC1 activity, potentially explaining the simultaneous activation of mTORC1 and the autophagy-lysosome pathway in senescent cells, where autophagic regulation of FLCN has been observed in cancer (Di Malta et al., 2017). TRAF3, a cytoplasmic E3 ubiquitin ligase, regulates various signaling pathways, including NF-κB, mitogen-activated protein kinase (MAPK), and interferon regulatory factor (IRF) pathways. It plays a significant role in controlling numerous biological processes in both immune and non-immune cell types (Gao P et al., 2021; Kang et al., 2021). Notably, TRAF3 is a well-known negative regulator of the non-canonical NF-κB pathway, which is activated

through a limited number of TNF superfamily receptors, indicating its specific biological functions (Cildir et al.,2016; Sun et al., 2017; Dejardin et al., 2006). In the steady-state condition, NIK (NF-κB-inducing kinase), the key kinase in this pathway, remains undetectable due to TRAF3-mediated ubiquitination and degradation. However, upon stimulation, TRAF3 is degraded by the E3 ubiquitin ligase cIAP (cellular inhibitor of apoptosis), leading to NIK accumulation (Liao et al., 2004; Sun et al., 2010). This suggests that autophagic regulation of TRAF3 might contribute to maintaining the inflammatory phenotype of senescent cells over an extended period and could be another piece in the axis of SASP (Senescence-Associated Secretory Phenotype) regulation, similar to the autophagic regulation of GATA4 and cytoplasmic chromatin fragments like TNIP1. Since these autophagy substrates are not limited to senescence, studying their mechanisms will provide insights into the broader cellular context of autophagic regulation, extending beyond senescence and enhancing our understanding of the signaling network controlled by selective autophagy.

In conclusion, our study presents an integrated platform for the identification, validation, and characterization of autophagy substrate proteins. Through this platform, we have uncovered multiple autophagy substrate proteins that coordinate the homeostatic state of senescence. These newly discovered functions of autophagy, which resemble the well-known regulation by the UPS, provide insights into autophagy's contributions to senescence establishment and reveal vulnerabilities of senescent cells. Developing precise methods to modulate selective autophagy would open up possibilities for treating various age-related pathologies, including osteoarthritis, and represents a significant step forward in the field of senotherapy.

REFERENCE

Acosta, J.C., Banito, A., Wuestefeld, T., Georgilis, A., Janich, P., Morton, J.P., Athineos, D., Kang, T.W., Lasitschka, F., Andrulis, M., et al. (2013). A complex secretory program orchestrated by the inflammasome controls paracrine senescence. Nat Cell Biol 15, 978-990.

Akbar, N., Nanda, S., Belch, J., Cohen, P., and Khan, F. (2015). An important role for A20-binding inhibitor of nuclear factor-kB-1 (ABIN1) in inflammation-mediated endothelial dysfunction: an in vivo study in ABIN1 (D485N) mice. Arthritis Res Ther 17, 22.

Anding, A.L., and Baehrecke, E.H. (2017). Cleaning House: Selective Autophagy of Organelles. Dev Cell 41, 10-22.

Bae, S.H., Sung, S.H., Oh, S.Y., Lim, J.M., Lee, S.K., Park, Y.N., Lee, H.E., Kang, D., and Rhee, S.G. (2013). Sestrins activate Nrf2 by promoting p62-dependent autophagic degradation of Keap1 and prevent oxidative liver damage. Cell Metab 17, 73-84.

Baker D.J., Childs B.G., Durik M., Wijers M.E., Sieben C.J., Zhong J., Saltness R.A., Jeganathan K.B., Verzosa G.C., Pezeshki A., et al. Naturally occurring p16(Ink4a)-positive cells shorten healthy lifespan. Nature. 2016;530:184-189.

Baker D.J., Wijshake T., Tchkonia T., LeBrasseur N.K., Childs B.G., van de Sluis B., Kirkland J.L., van Deursen J.M. Clearance of p16Ink4a-positive senescent cells delays ageing-associated disorders. Nature. 2011;479:232-236.

Basisty, N., Kale, A., Jeon, O.H., Kuehnemann, C., Payne, T., Rao, C., Holtz, A., Shah, S., Sharma, V., Ferrucci, L., et al. (2020). A proteomic atlas of senescence-associated secretomes for aging biomarker development. Plos Biol 18.

Behrends, C., Sowa, M.E., Gygi, S.P., and Harper, J.W. (2010).

Network organization of the human autophagy system. Nature 466, 68-U84.
Campisi, J., Kapahi, P., Lithgow, G.J., Melov, S., Newman, J.C., and Verdin, E. (2019). From discoveries in ageing research to therapeutics for healthy ageing. Nature 571, 183-192.
Cate, J.H. (2017). Human eIF3: from 'blobology' to biological insight. Philos Trans R Soc Lond B Biol Sci 372.
Chan, A.S.L., and Narita, M. (2019). Short-term gain, long-term pain: the senescence life cycle and cancer. Genes Dev 33, 127-143.
Chien, Y., Scuoppo, C., Wang, X., Fang, X., Balgley, B., Bolden, J.E., Premsrirut, P., Luo, W., Chicas, A., Lee, C.S., et al. (2011). Control of the senescence-associated secretory phenotype by NF-kappaB promotes senescence and enhances chemosensitivity. Genes Dev 25, 2125-2136.
Childs B.G., Durik M., Baker D.J., van Deursen J.M. Cellular senescence in aging and age-related disease: from mechanisms to therapy. Nat Med. 2015;21:1424-1435.
Childs, B.G., Gluscevic, M., Baker, D.J., Laberge, R.M., Marquess, D., Dananberg, J., and van Deursen, J.M. (2017). Senescent cells: an emerging target for diseases of ageing. Nat Rev Drug Discov 16, 718-735.
Cildir, G., Low, K. C. & Tergaonkar, V. Noncanonical NF-kappaB signaling in health and disease. Trends Mol. Med 22, 414-429 (2016).
Coppe, J.P., Patil, C.K., Rodier, F., Sun, Y., Munoz, D.P., Goldstein, J., Nelson, P.S., Desprez, P.Y., and Campisi, J. (2008). Senescence-associated secretory phenotypes reveal cell-nonautonomous functions of oncogenic RAS and the p53 tumor suppressor. Plos Biol 6, 2853-2868.
De Cecco, M., Ito, T., Petrashen, A.P., Elias, A.E., Skvir, N.J., Criscione, S.W., Caligiana, A., Brocculi, G., Adney, E.M., Boeke, J.D.,

et al. (2019). L1 drives IFN in senescent cells and promotes age-associated inflammation. Nature 566, 73-+.
Dejardin, E. The alternative NF-kappaB pathway from biochemistry to biology: pitfalls and promises for future drug development. Biochem. Pharmacol. 72, 1161-1179 (2006).
Demaria M., O' Leary M.N., Chang J., Shao L., Liu S., Alimirah F., Koenig K., Le C., Mitin N., Deal A.M., et al. Cellular senescence promotes adverse effects of chemotherapy and cancer relapse. Cancer Discov. 2017;7:165-176.
Di Malta, Chiara, et al. "Transcriptional activation of RagD GTPase controls mTORC1 and promotes cancer growth." Science 356.6343 (2017): 1188-1192.
Dorr J.R., Yu Y., Milanovic M., Beuster G., Zasada C., Dabritz J.H., Lisec J., Lenze D., Gerhardt A., Schleicher K., et al. Synthetic lethal metabolic targeting of cellular senescence in cancer therapy. Nature. 2013;501:421-425.
Dou, Z., Xu, C., Donahue, G., Shimi, T., Pan, J.A., Zhu, J., Ivanov, A., Capell, B.C., Drake, A.M., Shah, P.P., et al. (2015). Autophagy mediates degradation of nuclear lamina. Nature 527, 105-109.
Emanuele, M.J., Elia, A.E., Xu, Q., Thoma, C.R., Izhar, L., Leng, Y., Guo, A., Chen, Y.N., Rush, J., Hsu, P.W., et al. (2011). Global identification of modular cullin-RING ligase substrates. Cell 147, 459-474.
Galluzzi, L., Baehrecke, E.H., Ballabio, A., Boya, P., Bravo-San Pedro, J.M., Cecconi, F., Choi, A.M., Chu, C.T., Codogno, P., Colombo, M.I., et al. (2017). Molecular definitions of autophagy and related processes. Embo J 36, 1811-1836.
Gao, P., Ma, X., Yuan, M., Yi, Y., Liu, G., Wen, M., Jiang, W., Ji, R., Zhu, L., Tang, Z., Yu, Q., Xu, J., Yang, R., Xia, S., Yang, M., Pan, J., Yuan, H., & An, H. (2021). E3 ligase Nedd4l promotes antiviral innate immunity by catalyzing K29-linked cysteine ubiquitination of

TRAF3. Nature communications, 12(1), 1194.
Garcia-Prat, L., Martinez-Vicente, M., Perdiguero, E., Ortet, L., Rodriguez-Ubreva, J., Rebollo, E., Ruiz-Bonilla, V., Gutarra, S., Ballestar, E., Serrano, A.L., et al. (2016). Autophagy maintains stemness by preventing senescence. Nature 529, 37-42.
Gatica, D., Lahiri, V., and Klionsky, D.J. (2018). Cargo recognition and degradation by selective autophagy. Nat Cell Biol 20, 233-242.
Georgilis, A., Klotz, S., Hanley, C.J., Herranz, N., Weirich, B., Morancho, B., Leote, A.C., D'Artista, L., Gallage, S., Seehawer, M., et al. (2018). PTBP1-Mediated Alternative Splicing Regulates the Inflammatory Secretome and the Pro-tumorigenic Effects of Senescent Cells. Cancer Cell 34, 85-102 e109.
Gewirtz, D.A. (2013). Autophagy and senescence: a partnership in search of definition. Autophagy 9, 808-812.
Gorgoulis, V., Adams, P.D., Alimonti, A., Bennett, D.C., Bischof, O., Bishop, C., Campisi, J., Collado, M., Evangelou, K., Ferbeyre, G., et al. (2019). Cellular Senescence: Defining a Path Forward. Cell 179, 813-827.
G'Sell, R.T., Gaffney, P.M., and Powell, D.W. (2015). A20-Binding Inhibitor of NF-kappaB Activation 1 is a Physiologic Inhibitor of NF-kappaB: A Molecular Switch for Inflammation and Autoimmunity. Arthritis Rheumatol 67, 2292-2302.
He S., Sharpless N.E. Senescence in health and disease. Cell. 2017;169:1000-1011.
Helman A., Klochendler A., Azazmeh N., Gabai Y., Horwitz E., Anzi S., Swisa A., Condiotti R., Granit R.Z., Nevo Y., et al. p16(Ink4a)-induced senescence of pancreatic beta cells enhances insulin secretion. Nat Med. 2016;22:412-420.
Heo, J.M., Ordureau, A., Paulo, J.A., Rinehart, J., and Harper, J.W. (2015). The PINK1-PARKIN Mitochondrial Ubiquitylation Pathway Drives a Program of OPTN/NDP52 Recruitment and TBK1

Activation to Promote Mitophagy. Mol Cell 60, 7−20.
Hernandez−Segura, A., de Jong, T.V., Melov, S., Guryev, V., Campisi, J., and Demaria, M. (2017). Unmasking Transcriptional Heterogeneity in Senescent Cells. Curr Biol 27, 2652−2660 e2654.
Hernandez−Segura, A., Nehme, J., and Demaria, M. (2018). Hallmarks of Cellular Senescence. Trends Cell Biol 28, 436−453.
Herranz, N., and Gil, J. (2018). Mechanisms and functions of cellular senescence. J Clin Invest 128, 1238−1246.
Herranz, N., Gallage, S., Mellone, M., Wuestefeld, T., Klotz, S., Hanley, C.J., Raguz, S., Acosta, J.C., Innes, A.J., Banito, A., et al. (2015). mTOR regulates MAPKAPK2 translation to control the senescence−associated secretory phenotype. Nat Cell Biol 17, 1205−+.
Hipp, M.S., Kasturi, P., and Hartl, F.U. (2019). The proteostasis network and its decline in ageing. Nat Rev Mol Cell Biol 20, 421−435.
"Horikawa, I., Fujita, K., Jenkins, L. M., Hiyoshi, Y., Mondal, A. M., Vojtesek, B., et al.
(2014). Autophagic degradation of the inhibitory p53 isoform Delta133p53alpha as a regulatory
mechanism for p53−mediated senescence. Nature Communications, 5, 4706."
Huang da, W., Sherman, B.T., and Lempicki, R.A. (2009). Bioinformatics enrichment tools: paths toward the comprehensive functional analysis of large gene lists. Nucleic Acids Res 37, 1−13.
Ichimura, Y., and Komatsu, M. (2018). Activation of p62/SQSTM1−Keap1−Nuclear Factor Erythroid 2−Related Factor 2 Pathway in Cancer. Front Oncol 8, 210.
Ichimura, Y., Waguri, S., Sou, Y.S., Kageyama, S., Hasegawa, J., Ishimura, R., Saito, T., Yang, Y., Kouno, T., Fukutomi, T., et al. (2013). Phosphorylation of p62 activates the Keap1−Nrf2 pathway

during selective autophagy. Mol Cell 51, 618-631.
Iconomou, M., and Saunders, D.N. (2016). Systematic approaches to identify E3 ligase substrates. Biochem J 473, 4083-4101.
Ivanov, A., Pawlikowski, J., Manoharan, I., van Tuyn, J., Nelson, D.M., Rai, T.S., Shah, P.P., Hewitt, G., Korolchuk, V.I., Passos, J.F., et al. (2013). Lysosome-mediated processing of chromatin in senescence. J Cell Biol 202, 129-143.
Jeon, O.H., Kim, C., Laberge, R.M., Demaria, M., Rathod, S., Vasserot, A.P., Chung, J.W., Kim, D.H., Poon, Y., David, N., et al. (2017). Local clearance of senescent cells attenuates the development of post-traumatic osteoarthritis and creates a pro-regenerative environment. Nat Med 23, 775-+.
Johansen, T., and Lamark, T. (2020). Selective Autophagy: ATG8 Family Proteins, LIR Motifs and Cargo Receptors. J Mol Biol 432, 80-103.
Kang, C. (2019). Senolytics and Senostatics: A Two-Pronged Approach to Target Cellular Senescence for Delaying Aging and Age-Related Diseases. Mol Cells 42, 821-827.
Kang, C., and Elledge, S.J. (2016). How autophagy both activates and inhibits cellular senescence. Autophagy 12, 898-899.
Kang, C., Xu, Q.K., Martin, T.D., Li, M.Z., Demaria, M., Aron, L., Lu, T., Yankner, B.A., Campisi, J., and Elledge, S.J. (2015). The DNA damage response induces inflammation and senescence by inhibiting autophagy of GATA4. Science 349.
Kang, D., Shin, J., Cho, Y., Kim, H.S., Gu, Y.R., Kim, H., You, K.T., Chang, M.J., Chang, C.B., Kang, S.B., et al. (2019). Stress-activated miR-204 governs senescent phenotypes of chondrocytes to promote osteoarthritis development. Sci Transl Med 11.
Kang, J., Pang, Z., Zhou, Z., Li, X., Liu, S., Cheng, J., Liu, P., Tan, W., Wang, Z., & Wang, T. (2021). Enterovirus D68 Protease 2Apro Targets TRAF3 To Subvert Host Innate Immune Responses.

Journal of virology, 95(3), e01856-20.
Kastenhuber, E.R., and Lowe, S.W. (2017). Putting p53 in Context. Cell 170, 1062-1078.
Kaushik, S., and Cuervo, A.M. (2015). Proteostasis and aging. Nat Med 21, 1406-1415.
Kirkland, J.L., and Tchkonia, T. (2017). Cellular Senescence: A Translational Perspective. EBioMedicine 21, 21-28.
Komatsu, M., Kurokawa, H., Waguri, S., Taguchi, K., Kobayashi, A., Ichimura, Y., Sou, Y.S., Ueno, I., Sakamoto, A., Tong, K.I., et al. (2010). The selective autophagy substrate p62 activates the stress responsive transcription factor Nrf2 through inactivation of Keap1. Nat Cell Biol 12, 213-U217.
"Kroemer, G., Marino, G., & Levine, B. (2010). Autophagy and the integrated stress response.
Molecular Cell, 40(2), 280–293."
Kuilman T., Michaloglou C., Mooi W.J., Peeper D.S. The essence of senescence. Genes Dev. 2010;24:2463–2479.
Kwon, Y., Kim, J.W., Jeoung, J.A., Kim, M.S., and Kang, C. (2017). Autophagy Is Pro-Senescence When Seen in Close-Up, but Anti-Senescence in Long-Shot. Mol Cells 40, 607-612.
Laberge, R.M., Sun, Y., Orjalo, A.V., Patil, C.K., Freund, A., Zhou, L.L., Curran, S.C., Davalos, A.R., Wilson-Edell, K.A., Liu, S., et al. (2015). MTOR regulates the pro-tumorigenic senescence-associated secretory phenotype by promoting IL1A translation. Nat Cell Biol 17, 1049-U1416.
Leidal, A.M., Levine, B., and Debnath, J. (2018). Autophagy and the cell biology of age-related disease. Nat Cell Biol 20, 1338-1348.
Lessard, F., Igelmann, S., Trahan, C., Huot, G., Saint-Germain, E., Mignacca, L., Del Toro, N., Lopes-Paciencia, S., Le Calve, B., Montero, M., et al. (2018). Senescence-associated ribosome biogenesis defects contributes to cell cycle arrest through the Rb

pathway. Nat Cell Biol 20, 789−+.
"Levine, B., & Klionsky, D. J. (2004). Development by self-digestion: Molecular mechanisms
and biological functions of autophagy. Developmental Cell, 6(4), 463-477."
Levine, B., and Kroemer, G. (2019). Biological Functions of Autophagy Genes: A Disease Perspective. Cell 176, 11−42.
Li, Jingxian, et al. "Post−translational modifications in liquid−liquid phase separation: a comprehensive review." Molecular Biomedicine 3.1 (2022): 13.
Liao, G., Zhang, M., Harhaj, E. W. & Sun, S. C. Regulation of the NF−kappaB−inducing kinase by tumor necrosis factor receptor−associated factor 3−induced degradation. J. Biol. Chem. 279, 26243-26250 (2004).
Lopez−Otin C., Blasco M.A., Partridge L., Serrano M., Kroemer G. The hallmarks of aging. Cell. 2013;153:1194-1217.
Luo, J., Solimini, N.L., and Elledge, S.J. (2009). Principles of cancer therapy: oncogene and non−oncogene addiction. Cell 136, 823−837.
McHugh D., Gil J. Senescence and aging: causes, consequences, and therapeutic avenues. J Cell Biol. 2018;217:65-77.
Miller, D.R., and Thorburn, A. (2021). Autophagy and organelle homeostasis in cancer. Dev Cell.
Mizushima, N., and Komatsu, M. (2011). Autophagy: renovation of cells and tissues. Cell 147, 728−741.
Mosteiro L., Pantoja C., Alcazar N., Marion R.M., Chondronasiou D., Rovira M., Fernandez−Marcos P.J., Munoz−Martin M., Blanco−Aparicio C., Pastor J., et al. Tissue damage and senescence provide critical signals for cellular reprogramming in vivo. Science. 2016;354:aaf4445.
Munoz−Espin D., Serrano M. Cellular senescence: from physiology to pathology. Nat Rev Mol Cell Biol. 2014;15:482-496.

Narita, M., Young, A.R., Arakawa, S., Samarajiwa, S.A., Nakashima, T., Yoshida, S., Hong, S., Berry, L.S., Reichelt, S., Ferreira, M., et al. (2011). Spatial coupling of mTOR and autophagy augments secretory phenotypes. Science 332, 966-970.

Newman, A.C., Kemp, A.J., Drabsch, Y., Behrends, C., and Wilkinson, S. (2017). Autophagy acts through TRAF3 and RELB to regulate gene expression via antagonism of SMAD proteins. Nat Commun 8.

Niedernhofer L.J., Robbins P.D. Senotherapeutics for healthy ageing. Nat Rev Drug Discov. 2018;17:377.

Noda, N. N., Wang, Z., & Zhang, H. (2020). Liquid-liquid phase separation in autophagy. The Journal of cell biology, 219(8), e202004062.

Olsvik, H.L., Lamark, T., Takagi, K., Larsen, K.B., Evjen, G., Overvatn, A., Mizushima, T., and Johansen, T. (2015). FYCO1 Contains a C-terminally Extended, LC3A/B-preferring LC3-interacting Region (LIR) Motif Required for Efficient Maturation of Autophagosomes during Basal Autophagy. J Biol Chem 290, 29361-29374.

Pohl, C., and Dikic, I. (2019). Cellular quality control by the ubiquitin-proteasome system and autophagy. Science 366, 818-+.

Ramos, Y.F., den Hollander, W., Bovee, J.V., Bomer, N., van der Breggen, R., Lakenberg, N., Keurentjes, J.C., Goeman, J.J., Slagboom, P.E., Nelissen, R.G., et al. (2014). Genes involved in the osteoarthritis process identified through genome wide expression analysis in articular cartilage; the RAAK study. PLoS One 9, e103056.

Richter, B., Sliter, D.A., Herhaus, L., Stolz, A., Wang, C., Beli, P., Zaffagnini, G., Wild, P., Martens, S., Wagner, S.A., et al. (2016). Phosphorylation of OPTN by TBK1 enhances its binding to Ub chains and promotes selective autophagy of damaged mitochondria. Proc Natl Acad Sci U S A 113, 4039-4044.

Ritschka B., Storer M., Mas A., Heinzmann F., Ortells M.C., Morton J.P., Sansom O.J., Zender L., Keyes W.M. The senescence-associated secretory phenotype induces cellular plasticity and tissue regeneration. Genes Dev. 2017;31:172-183.
Rual, J.F., Venkatesan, K., Hao, T., Hirozane-Kishikawa, T., Dricot, A., Li, N., Berriz, G.F., Gibbons, F.D., Dreze, M., Ayivi-Guedehoussou, N., et al. (2005). Towards a proteome-scale map of the human protein-protein interaction network. Nature 437, 1173-1178.
Salama R., Sadaie M., Hoare M., Narita M. Cellular senescence and its effector programs. Genes Dev. 2014;28:99-114.
Sanchez-Martin, P., and Komatsu, M. (2020). Physiological Stress Response by Selective Autophagy. J Mol Biol 432, 53-62.
Shen, D., Coleman, J., Chan, E., Nicholson, T.P., Dai, L., Sheppard, P.W., and Patton, W.F. (2011). Novel cell- and tissue-based assays for detecting misfolded and aggregated protein accumulation within aggresomes and inclusion bodies. Cell Biochem Biophys 60, 173-185.
Soto-Gamez A., Demaria M. Therapeutic interventions for aging: the case of cellular senescence. Drug Dis Today. 2017;22:786-795.
Subramanian, A., Tamayo, P., Mootha, V.K., Mukherjee, S., Ebert, B.L., Gillette, M.A., Paulovich, A., Pomeroy, S.L., Golub, T.R., Lander, E.S., et al. (2005). Gene set enrichment analysis: a knowledge-based approach for interpreting genome-wide expression profiles. Proc Natl Acad Sci U S A 102, 15545-15550.
Sun, S. C. Controlling the fate of NIK: a central stage in noncanonical NF-kappaB signaling. Sci. Signal 3, pe18 (2010).
Sun, S.-C. The non-canonical NF-κB pathway in immunity and inflammation. Nat. Rev. Immunol. 17, 545 (2017).
Taguchi, K., Fujikawa, N., Komatsu, M., Ishii, T., Unno, M., Akaike, T., Motohashi, H., and Yamamoto, M. (2012). Keap1 degradation by

autophagy for the maintenance of redox homeostasis. Proc Natl Acad Sci U S A 109, 13561–13566.
Tchkonia T., Zhu Y., van Deursen J., Campisi J., Kirkland J.L. Cellular senescence and the senescent secretory phenotype: therapeutic opportunities. J Clin Invest. 2013;123:966–972.
Torres, E.M., Dephoure, N., Panneerselvam, A., Tucker, C.M., Whittaker, C.A., Gygi, S.P., Dunham, M.J., and Amon, A. (2010). Identification of aneuploidy–tolerating mutations. Cell 143, 71–83.
van Deursen, J.M. (2019). Senolytic therapies for healthy longevity. Science 364, 636–637.
White, E. (2015). The role for autophagy in cancer. J Clin Invest 125, 42–46.
Wiley, C.D., and Campisi, J. (2016). From Ancient Pathways to Aging Cells–Connecting Metabolism and Cellular Senescence. Cell Metab 23, 1013–1021.
Xu, C., Wang, L., Fozouni, P., Evjen, G., Chandra, V., Jiang, J., Lu, C., Nicastri, M., Bretz, C., Winkler, J.D., et al. (2020). SIRT1 is downregulated by autophagy in senescence and ageing. Nat Cell Biol 22, 1170–1179.
Yen, H.C.S., Xu, Q.K., Chou, D.M., Zhao, Z.M., and Elledge, S.J. (2008). Global Protein Stability Profiling in Mammalian Cells. Science 322, 918–923.
Young, A.R., Narita, M., Ferreira, M., Kirschner, K., Sadaie, M., Darot, J.F., Tavare, S., Arakawa, S., Shimizu, S., Watt, F.M., et al. (2009). Autophagy mediates the mitotic senescence transition. Genes Dev 23, 798–803.

국문 초록

이영현
생명과학부 대학원
서울대학교

세포 노화는 개체 노화와 관련된 복잡한 스트레스 반응입니다. 오토파지가 세포 노화를 억제할 수 있다는 것이 잘 알려져 있지만, 역설적으로 세포 노화의 완전한 확립에는 필수적이기도 합니다. 오토파지의 항-세포 노화 역할은 잘 알려져 있지만, 오토파지가 세포 노화 확립에 어느 정도 기여하며 어떤 기작을 통해 작용하는지는 잘 알려져 있지 않습니다. 본 연구에서는, 세포 노화의 여러 조절자들의 선택적 자가포식이 세포 노화의 항상성 상태를 정밀하게 조정한다는 것을 보여줍니다. 오토파지 구성 요소들에 대한 단백질체 분석과 단백질 안정성 프로파일링을 결합하여 여러 세포 노화 관련 프로세스에 관여하는 오토파지 기질 단백질을 동정하였습니다. KEAP1의 선택적 오토파지는 세포 노화 과정에서 산화 환원 항상성을 촉진합니다. 또한, 선택적 오토파지는 세포 내 번역 기계 구성 요소를 제한하여 노화 세포의 단백질 독성 스트레스를 완화합니다. 마지막으로, TNIP1의 선택적 오토파지는 세포 노화 관련 염증을 증가시킵니다. 이러한 선택적 오토파지 네트워크는 인간 골관절염의 생체 내 노화 과정에서 실제로 작동하는 것으로 보입니다. 결과적으로 본 연구는 단백질 안정성 조절을 통해 오토파지가 세포 노화의 스트레스 서포트 네트워크를 조정할 수 있다는 것을 제안하고, 오토파지와 세포 노화라는 두 가지 중요한 노화 관련 과정 사이의 얽힌 관계를 밝힙니다.

주요어 : 세포 노화, 선택적 오토파지, 스트레스 반응, 산화 스트레스, 단백질 독성, 염증반응

학 번 : 2018-25197